NAG3-2930

UNIVERSITY OF FLORIDA

PROJECT TITLE: FLUID DISTRIBUTION FOR IN-SPACE CRYOGENIC PROPULSION

Task PI: Dr. William Lear, Department of Mechanical and Aerospace Engineering

PROJECT GOALS

The ultimate goal of this task is to enable the use of a single supply of cryogenic propellants for three distinct spacecraft propulsion missions: main propulsion, orbital maneuvering, and attitude control. A fluid distribution system is sought which allows large propellant flows during the first two missions while still allowing control of small propellant flows during attitude control. Existing research has identified the probable benefits of a combined thermal management/power/fluid distribution system based on the Solar Integrated Thermal Management and Power (SITMAP) cycle. Both a numerical model and an experimental model are constructed in order to predict the performance of such an integrated thermal management/propulsion system. This research task provides a numerical model and an experimental apparatus which will simulate an integrated thermal/power/fluid management system based on the SITMAP cycle, and assess its feasibility for various space missions. Various modifications are done to the cycle, such as the addition of a regeneration process that allows heat to be transferred into the working fluid prior to the solar collector, thereby reducing the collector size and weight. Fabri choking analysis was also accounted for. Finally the cycle is to be optimized for various space missions based on a mass based figure of merit, namely the System Mass Ratio (SMR).

The theoretical and experimental results from these models are be used to develop a design code (JETSIT code) which is able to provide design parameters for such a system, over a range of cooling loads, power generation, and attitude control thrust levels. The performance gains and mass savings will be compared to those of existing spacecraft systems.

OVERVIEW

After an extensive review of fluid distribution technology, it was decided that the most promising avenue of research for this project would involve a combined thermal management/power generation/ propellant distribution system that is based on the SITMAP cycle. The SITMAP cycle integrates a vapor compression (refrigeration) thermal management subsystem, which uses a jet pump rather than a compressor, and a power subsystem that is essentially a Rankine cycle in which the jet pump replaces a turbine. In the current implementation, the working fluid would be one or more cryogenic propellants. The SITMAP cycle's physical setup within a spacecraft could provide a constant flow of propellant to the spacecraft's extremities, and this flow could easily be tapped into at an ideal location in order to bleed off propellant for attitude control purposes.

This leads to another benefit of the SITMAP cycle for fluid distribution purposes. Because of the SITMAP cycle operational characteristics; there is a region in the cycle where pressurized superheated vapor exists – after the waste heat recovery unit and/or solar collector and before the turbine inlet. This part of the cycle could easily be tapped and the superheated vapor used directly as a thrust source for attitude control.

Using the fluid in its highest energy state within the SITMAP cycle would optimize its effectiveness as a propellant and could eliminate the need for any type of burner, resulting in a simple and more reliable means of spacecraft attitude control. Figure 1 illustrates such a system.

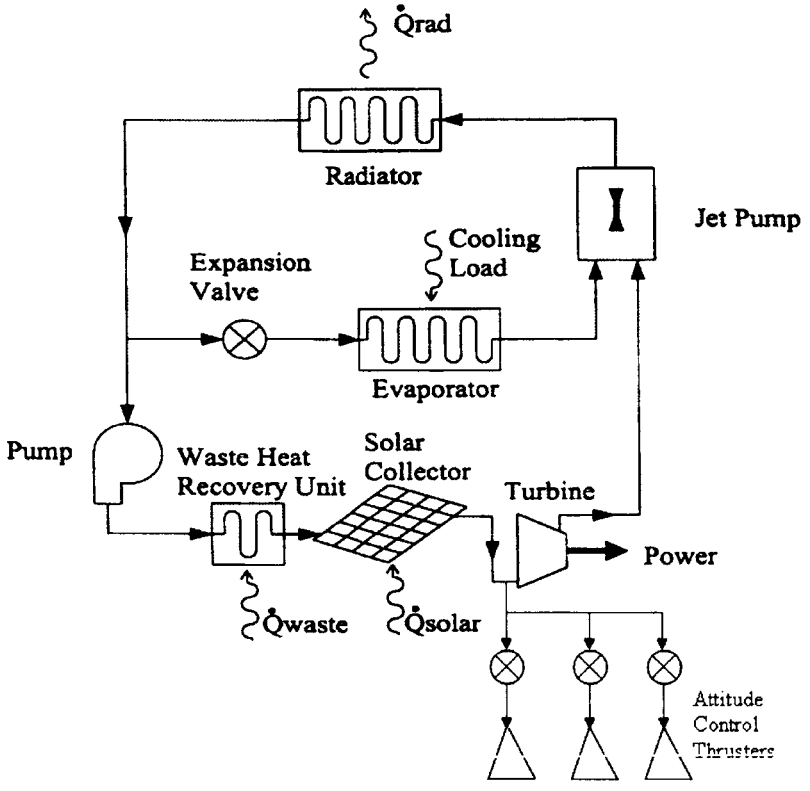

Figure 1: SITMAP-based integrated thermal management/power generation/ propellant delivery system.

A parallel University of Florida research project has focused on the numerical and experimental analysis of a SITMAP cycle that does not include a mass flow bleed. The results of this parallel research have been and will continue to be utilized in the development of the modified SITMAP cycle (with a mass flow bleed, or bleeds). Both computer codes and experimental apparatus have been constructed which will be progressively modified for use in the analysis of a modified SITMAP cycle.

Research work done on the SITMAP cycle is comprised of two parts, an analytical part, and an experimental part. Following are summaries of both parts of the program.

ANALYTICAL PROGRAM

The analytical part went through different stages starting with the development of a computer code (JetSit, which is short for Jet-pump and SITMAP) for the thermodynamic simulation of the cycle. An expression was then needed to measure the mass based performance of the cycle. For that purpose a System Mass Ratio (SMR) expression was derived and incorporated in the simulation code JetSit. Further development of the code involved incorporating thermodynamic properties software to calculate thermodynamic properties instead of the use of a data file. The software used is called REFPROP and is made by NIST. Recuperation was then included in the

SITMAP cycle as an effort to decrease the weight of the system (see Figure 2). Fabri choking is an important phenomenon that might take place in the mixing chamber of the Jet-pump. Fabri choking refers to conditions when the primary flow expands in the mixing chamber constricting the available flow area for the secondary stream, causing it to accelerate. It is possible for the secondary stream to reach sonic velocity, therefore causing the secondary mass flow rate to become independent of downstream conditions. The Fabri choking analysis was included in the JetSit cycle simulation code to make sure that the input entrainment ratios are physically possible.

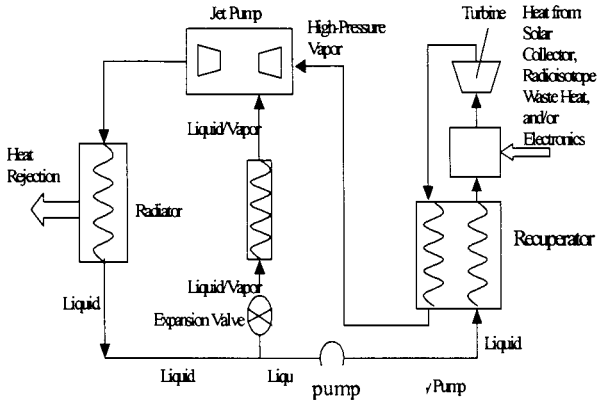

Figure 2. Schematic of the Solar Integrated Thermal Management and Power (SITMAP) cycle with regeneration

The current and most recent stage of the analytical part in the SITMAP program is the optimization of the cycle to minimize the mass for different space missions. To achieve this, an optimization program was incorporated in the cycle simulation code. The optimization routine is written by Dr. Leon Lasdon of the University of Texas in Austin and it utilizes a Generalized Reduced Gradient algorithm, and is hence called GRG2.

The most results of the analytical part of the program are presented below. Appendix A includes the more recent work that hasn't been published yet, including the Fabri choking, and optimization analyses.

Results of the preceding analysis are presented in Tables 1 through 5. Each of the five sets has the same primary inlet pressure, while varying the secondary pressure. The ratio $\left(P_{pi}/P_{si}\right)_{bo}$ is the break-off pressure ratio. This is the ratio below which the flow operates either in the mixed regime or in the saturated supersonic regime (inlet choking regime), and above which the flow operates either in the mixed regime or the supersonic regime (Fabri choking regime).

There are some general trends that can bee seen in all data sets. First, once the pressure ratio Ppi/Psi is larger than its break-off value, ϕFabri becomes the upper limit (supersonic flow regime). When Ppi/Psi is less than its break-off value the limiting value for the entrainment ratio is ϕinlet choke (saturated supersonic regime). For any line of data in all data sets, if the

entrainment ratio drops below the limiting value, the jet-pump will be operating in the "mixed regime", where ϕ is dependent on the downstream conditions (or the back pressure). It should also be noted that as long as the ratio Ppi/Psi is above the break-off ratio, the pressure ratio Pse/Pne drops below unity, which is important for the primary flow to expand into the secondary causing Fabri choking to take place.

The second general trend is the increase of the limiting value of the entrainment ratio with higher secondary pressure. This should be expected because since the primary inlet pressure is fixed, a higher secondary stagnation pressure corresponds to a lower backpressure. The lower backpressure allows for more secondary flow entrainment before choking occurs.

Data sets 1 to 3 show the effect of the ratio of primary and secondary stagnation temperatures on the maximum entrainment ratio. Figure 3 is a graphical representation of Tables 1 to 3. It can be seen that higher entrainment ratios can be achieved for higher stagnation temperature ratios. The effect of Tpi/Tsi on maximum ϕ is less significant at higher Ppi/Psi ratios, but the same trend still holds.

Tables 3 and 4 show the effect of varying the primary nozzle geometry. Figure 4 shows the same effect in graphical form. It can be seen that lower Ant/Ane ratios (i.e. higher Mne) allow more secondary flow entrainment. This makes sense, since the entrainment mechanism is by viscous interaction between the secondary and primary streams. Therefore, faster primary flow should be able to entrain more secondary flow.

Tables 4 and 5 show the effect of the area ratio Ane/Ase. Figure 5 shows that lower primary-to-secondary area ratios allow for more entrainment. This trend is expected since a lower area ratio means more area for the secondary flow and thus more secondary mass flow rate. Figure 6 shows the variation of the compression ratio with Ppi/Psi, for different jet-pump geometries. The compression ratio was calculated for maximum allowable entrainment ratio. It can be seen that as the ratio Ppi/Psi increases the compression ratio increases as well, which is expected.

Table 1: Data set # 1. Tpi = 200, Tsi = 100, Ant/Ane = 0.25, Ane/Ase = 0.1

Ppi	Psi	Ppi / Psi	PHlinlet	PHlfabri	Pse	Pse/Pne	(Ppi / Psi)bo	Pne
3200000	1600000	2	144.996		752031.170	7.30495	16.51	102948
3200000	1066666.667	3	85.465		766654.157	7.447		Mne
3200000	640000	5	11.1029		366170.684	3.55685		3.07605
3200000	320000	10	5.58389		169866.433	1.65002		
3200000	213333.3333	15	3.67901		113017.917	1.09781		
3200000	160000	20		2.683032	100556.41	0.97677		
3200000	128000	25		2.083661	86249.331	0.83779		
3200000	106666.6667	30		1.676613	76063.5258	0.73885		
3200000	91428.57143	35		1.383796	68217.1583	0.66264		
3200000	80000	40		1.164268	61920.2561	0.60147		
3200000	71111.11111	45		0.9936368	56761.0127	0.55136		
3200000	64000	50		0.8574538	52445.6223	0.50944		

Table 2: Data set # 2. Tpi = 100, Tsi = 100, Ant/Ane = 0.25, Ane/Ase = 0.1

Ppi	Psi	Ppi / Psi	PHIinlet	PHIfabri	Pse	Pse/Pne	(Ppi / Psi)bo	Pne
3200000	1600000	2	23.2413		752031.17	1.8963	4.62411	396579
3200000	1066666.667	3	13.6961		766654.081	1.93317		**Mne**
3200000	533333.3333	6		1.416579	376543.452	0.94948		2.57789
3200000	320000	10		0.6935064	264842.461	0.66782		
3200000	213333.3333	15		0.3329346	195893.323	0.49396		

Table 3: Data set # 3. Tpi = 400, Tsi = 100, Ant/Ane = 0.25, Ane/Ase = 0.1

P_{pi}	P_{si}	P_{pi}/P_{si}	$\phi_{inletchoke}$	ϕ_{Fabri}	ϕ	P_{se}/P_{ne}	P_{de}/P_{si}	$(P_{de}/P_{si})_{bo}$	P_{ne}
3200000	1600000.000	2	213.904		213.904	7.968	0	18.009699	94375.5814
3200000	640000.000	5	16.3609		16.36093	3.880	1.0485		M_{ne}
3200000	320000.000	10	8.22779		8.227792	1.800	1.19303		2.957
3200000	213333.333	15	5.42427		5.424266	1.198	1.34552		
3200000	160000.000	20		3.9997	3.999688	0.878	1.49797		
3200000	128000.000	25		3.1214	3.121448	0.773	1.65079		
3200000	106666.667	30		2.5321	2.532101	0.691	1.80439		
3200000	91428.571	35		2.1111	2.111098	0.627	1.95876		
3200000	80000.000	40		1.7958	1.795751	0.574	2.11383		
3200000	71111.111	45		1.5509	1.55091	0.543	2.26951		
3200000	64000.000	50		1.359	1.359	0.529	2.427		

Table 4: Data set # 4. Tpi = 400, Tsi = 100, Ant/Ane = 0.6, Ane/Ase = 0.1

P_{pi}	P_{si}	P_{pi}/P_{si}	$\phi_{inletchoke}$	ϕ_{Fabri}	ϕ	P_{se}/P_{ne}	P_{de}/P_{si}	$(P_{de}/P_{si})_{bo}$	P_{ne}
3200000	1600000.000	2	89.060			1.816	0.637	4.433	414056.656
3200000	640000.000	5		6.738	6.704	0.995	1.187		M_{ne}
3200000	320000.000	10		3.052	3.052	0.575	1.508		1.996
3200000	213333.333	15		1.810	1.810	0.420	1.842		
3200000	160000.000	20		1.194	1.194	0.334	2.183		
3200000	128000.000	25		0.832	0.832	0.278	2.527		
3200000	106666.667	30		0.594	0.594	0.239	2.876		
3200000	91428.571	35		0.428	0.428	0.210	3.228		
3200000	80000.000	40		0.305	0.305	0.187	3.583		
3200000	71111.111	45		0.2109	0.210895	0.165	3.941		
3200000	64000.000	50		0.137	0.137	0.153	4.301		

Table 5: Data set # 5. Tpi = 400, Tsi = 100, Ant/Ane = 0.25, Ane/Ase = 0.3

P_{pi}	P_{si}	P_{pi}/P_{si}	$\phi_{inletchoke}$	ϕ_{Fabri}	ϕ	P_{se}/P_{ne}	P_{de}/P_{si}	$(P_{de}/P_{si})_{bo}$	P_{ne}
3200000	1600000.000	2	71.301		71.301	7.968	0.715	18.009699	94375.581
3200000	640000.000	5	5.459		5.459	3.876	1.131		M_{ne}
3200000	320000.000	10	2.745		2.745	1.800	1.658		2.957
3200000	213333.333	15	1.810		1.810	1.198	2.185		
3200000	160000.000	20		1.008	1.008	1.112	2.712		
3200000	128000.000	25		0.789	0.789	0.942	3.108		
3200000	106666.667	30		0.631	0.631	0.850	3.507		
3200000	91428.571	35		0.513	0.513	0.772	3.908		
3200000	80000.000	40		0.421	0.421	0.706	4.311		
3200000	71111.111	45		0.401	0.401	0.650	4.561		
3200000	64000.000	50		0.348	0.348	0.602	4.716		

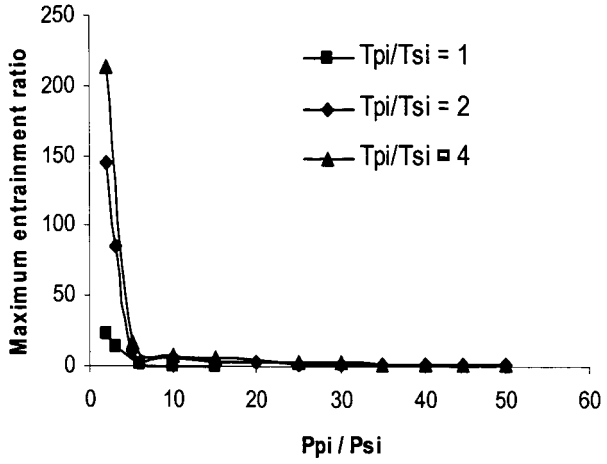

Figure 3: Maximum entrainment ratio variation versus the stagnation pressure ratio for different stagnation temperatures ratio. Based in ϕinletchoke and ϕFabri only

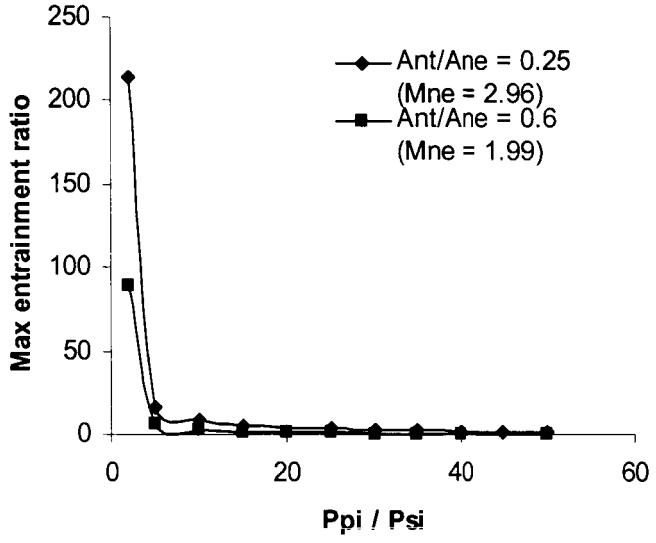

Figure 4: Maximum entrainment ratio variation versus the stagnation pressure ratio for different primary nozzle geometry. Based in ϕinletchoke, and ϕFabri only.

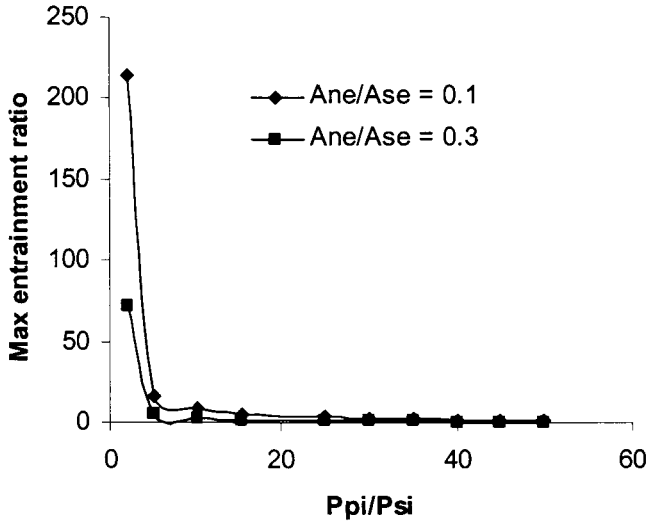

Figure 5: Maximum entrainment ratio variation versus the stagnation pressure ratio for different primary to secondary nozzles area ratios. Based in ϕinletchoke, and ϕFabri only.

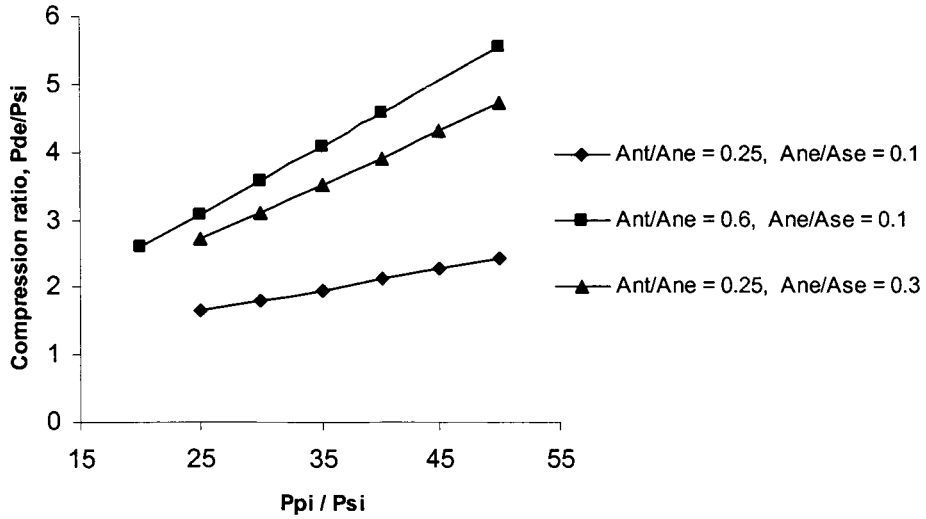

Figure 6: Compression ratio variation versus the stagnation pressure ratio

EXPERIMENTAL PROGRAM

The initial consideration in the experimental design process was to conceptually develop the best method of designing an ejector test rig that will be used to study the phenomena of two-phase flow mixing and compression. The primary design criterion established stated that the ejector primary and secondary nozzle inlet states were to be varied over a wide range of pressures, temperatures, and qualities in order to obtain a general database. The wide range of conditions is

vital in thoroughly investigating the effects to two-phase flow. A second design requirement dealt with the ability to change the area ratios of the primary and secondary inlet and outlet nozzles. The simulation program JetSit aided in the design of the ejector nozzles.

The first and most important design feature to accommodate was how to vary nozzle inlet states. Conceptually, some kind of loop must be designed to heat and cool the primary and secondary fluid flow. This heating and cooling process would necessarily incorporate the use of one or more heat exchangers. In order to gain control of the pressure, a valve (e.g. adjustable throttling valve) would be needed. The working fluid must also be circulated through the loop; consequently, a pump would be needed. All of the components listed above are basic parts of a system operating on the SITMAP cycle. From this reasoning it was resolved that in order to gain relatively good control of the experimental apparatus, all components of that system would need to be incorporated. Since it was deemed advantageous to also obtain system-level data for the SITMAP cycle, the choice of ejector rig design was driven towards implementing that cycle directly.

Another important design consideration was the selection of a working fluid for the two-phase flow ejector test rig. The main criterion used in the fluid selection involved the temperature and pressure ranges where the fluid would be in the two-phase region. For safety reasons it was decided that the loop would be operated near ambient temperature and pressure. Information about individual fluids was found by examining their Material Safety Data Sheets (MSDS). Those sheets provide information that cover hazardous ingredients, health effects, handling details, fire and explosion hazard data, first-aid procedures, and critical fluid properties. An important critical fluid property found in the MSDS is the boiling point of a fluid. Since the fluid will be operated in the two-phase region, only fluids with a boiling point temperature slightly above ambient temperature were considered. Based on this information, R-141b was selected. Once the working fluid was selected, the components were sized. Shown below in Figure 7 is a schematic of the final layout of the experimental setup.

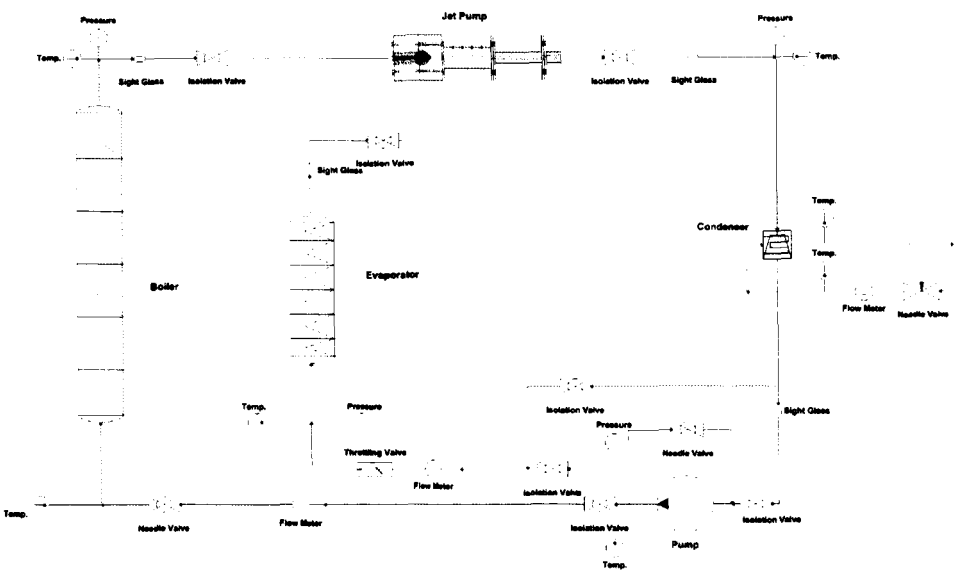

Figure 7. Schematic of the experimental testing apparatus

The most recently published paper on the experimental work is presented in appendix B.

APPENDIX A

NOMENCLATURE

Latin Symbols

A	cross-sectional area, m^2
a	speed of sound, m/s
COP	coefficient of performance, dimensionless
h	specific enthalpy, kJ/kg
M	Mach number, dimensionless
m	mass, kg
$\dot{m}$	mass flow rate, kg/s
P	pressure, MPa
P_r	compression ratio
Q`	heat transfer rate, kW
r	heat exchanger pressure ratio
T	temperature, °C
V	velocity, m/s
w`	work rate, kW

Greek Symbols

ϕ	entrainment ratio, $\dot{m}_s / \dot{m}_p$
ρ	density, kg/m^3

Subscripts

de	diffuser exit
ei	evaporator inlet
evap	evaporator
me	mixing chamber exit
n2	primary flow passage where fabri choking occurs
ne	primary nozzle exit
nt	primary nozzle throat
p	primary flow
pi	primary nozzle inlet
pe	pump exit
pump	mechanical pump
rad	radiator
re	radiator exit
s	secondary flow
s2	secondary flow passage where fabri choking occurs
sc	solar collector
se	secondary flow exit

si secondary flow inlet
ss state immediately downstream of shock wave
t turbine
ti turbine inlet
ts isentropic turbine exit state

FABRI CHOKING ANALYSIS

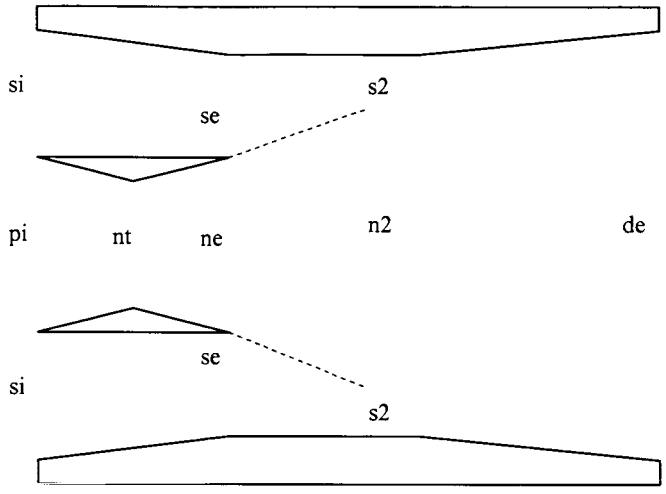

Figure 1. Schematic for the Jet-pump with constant area mixing, showing the Fabri choked state s2.

The momentum equation for the control volume over the mixing chamber can be written as

$$P_{se}A_{se} + P_{ne}A_{ne} - P_{s2}A_{s2} - P_{n2}A_{n2} = \dot{m}_p V_{n2} + \dot{m}_s V_{s2} - \dot{m}_p V_{ne} - \dot{m}_s V_{se} \tag{1a}$$

dividing by $\dot{m}_p$ yields

$$\frac{1}{\dot{m}_p}\left(P_{se}A_{se} + P_{ne}A_{ne} - P_{s2}A_{s2} - P_{n2}A_{n2}\right) = \left(V_{n2} - V_{ne}\right) + \phi_{Fabri}\left(V_{s2} - V_{se}\right) \tag{1b}$$

$$\therefore \phi_{Fabri} = \frac{\left(P_{se}A_{se} + P_{ne}A_{ne} - P_{s2}A_{s2} - P_{n2}A_{n2}\right)}{\dot{m}_p\left(V_{s2} - V_{se}\right)} - \frac{\left(V_{n2} - V_{ne}\right)}{\left(V_{s2} - V_{se}\right)} \tag{1c}$$

$$\therefore \phi_{Fabri} = \frac{\left(P_{se} + P_{ne}\dfrac{A_{ne}}{A_{se}} - P_{s2}\dfrac{A_{s2}}{A_{se}} - P_{n2}\dfrac{A_{n2}}{A_{ne}}\dfrac{A_{ne}}{A_{se}}\right)}{\rho_{ne}V_{ne}\dfrac{A_{ne}}{A_{se}}\left(V_{s2} - V_{se}\right)} - \frac{\left(V_{n2} - V_{ne}\right)}{\left(V_{s2} - V_{se}\right)} \tag{1d}$$

The iteration scheme starts by guessing a value for P_{se}, knowing that $s_{se} = s_{si}$, that defines the state (se). From the energy equation

$$V_{se} = \left[2(h_{si} - h_{se})\right]^{1/2} \tag{2}$$

then ϕ_{Fabri} can be calculated as

$$\phi_{Fabri} = \frac{\rho_{se} V_{se} A_{se}}{\rho_{ne} V_{ne} A_{ne}} \tag{3}$$

It should be noted that the area ratio A_{ne}/A_{se} is an input to the SITMAP code.

Then a guess is made for P_{s2}, and $s_{s2} = s_{se}$, that defines the state (s2). The velocity V_{s2} can be obtained from the energy equation between se and s2

$$V_{s2} = \left[2\left(h_{se} - h_{s2} + \frac{V_{se}^2}{2}\right)\right]^{1/2} \tag{4}$$

calculate $M_{s2} = \frac{V_{s2}}{a_{s2}}$, and check if it is equal to 1. If not another value for P_{s2} is guessed till $M_{s2} = 1$.

The area ratio A_{s2}/A_{se} can be calculated from the continuity equation between se and s2,

$$\frac{A_{s2}}{A_{se}} = \frac{\rho_{se} V_{se}}{\rho_{s2} V_{s2}} \tag{5}$$

knowing that for constant-area mixing $A_{ne} + A_{se} = A_{s2} + A_{n2}$, then

$$\frac{A_{n2}}{A_{ne}} = 1 + \frac{A_{se}}{A_{ne}} - \left(\frac{A_{s2}}{A_{se}} \frac{A_{se}}{A_{ne}}\right) \tag{6}$$

From equation 1d another value for ϕ_{Fabri} can be obtained. Iterate on P_{se} till the values for ϕ_{Fabri} from equations (1d) and (3) match.

ϕ_{Fabri} is the maximum possible entrainment ratio for a given geometry and inlet states. Therefore the simulation code JetSit sets $\phi = \phi_{Fabri}$, if the input value is greater than ϕ_{Fabri}.

OPTIMIZATION ANALYSIS

As mentioned before the optimization analysis is performed by incorporating a Generalized Reduced Gradient algorithm into the simulation code. The optimization algorithm is written by Dr, Leon Lasdon of the University of Texas in Austin, and is called GRG2.

All the input variables to the simulation program JetSit are the variables in the optimization process. A list of these variables is

- Jet-pump primary inlet pressure, P_{pi}
- Jet-pump primary inlet entropy, S_{pi}.
- Jet-pump secondary inlet pressure, P_{si}
- Jet-pump secondary entropy, S_{si}
- Jet-pump entrainment ratio, ϕ
- Area ratio Ant/Ane in the jet-pump primary nozzle
- Area ratio Ane/Ase in the jet-pump
- Turbine inlet pressure, P_{ti}

The constraints on the optimization process are

- $P_{ti} - P_{te} > 0$
- $P_{pe} - P_{re} > 0$
- $P_{pi} - P_{si} > 0$
- $P_{jpe} - P_{se} > 0$
- $Q_{evap} > 0$
- $Q_{boiler} > 0$
- $Q_{cond} > 0$
- SMR > 0 (objective function, to be minimized)

The objective function is the SMR, which is to be minimized for space applications. All the optimization variables are changed within a specified range to obtain the minimum value for the objective function, SMR, provided all the aforementioned constraints are satisfied.

UNIVERSITY OF FLORIDA

APPENDIX B

Proceedings of FEDSM'03
4TH ASME/JSME Joint Fluids Engineering Conference
Honolulu, Hawaii, USA, July 6–11, 2003

FEDSM2003-45703

Experimental Study of a Constant-Area Ejector with Two-Phase Fluids

J. A. Bray, W. E. Lear, and S. A. Sherif
Department of Mechanical and Aerospace Engineering
University of Florida
237 MAEB Bldg., P.O. Box 116300
Gainesville, Florida 32611-6300
Tel (352) 392-7821
Fax (352) 392-1071
E-mail: sasherif@ufl.edu

ABSTRACT

The authors are presently involved in developing a design code to optimize an active space thermal management system that includes as a key component an ejector, which operates with fluids in the two-phase regime. In order to validate this code, and for other applications of two-phase ejectors, a comprehensive experimental data set is needed for this device. This paper deals with the conceptual design and implementation of a constant-area ejector experimental rig intended to provide the required data set. The system has been designed to implement the same thermodynamic cycle as the proposed thermal management system, allowing a preliminary performance database to be developed upon testing, in addition to the ejector data. The ejector itself will be an interchangeable part in this system, allowing geometrical variables to be manipulated.

INTRODUCTION

Thermal management of spacecraft relies on rejection of heat via radiation, a process that can result in large radiator mass, depending upon the heat rejection temperature. For some missions, it is advantageous to incorporate an active thermal management system, allowing the heat rejection temperature to be greater than the load temperature. This allows a reduction of radiator mass at the expense of additional system complexity. A particular type of active thermal management system is based on a thermodynamic cycle, developed by the authors, called the Solar Integrated Thermal Management and Power (SITMAP) cycle. This system has been a focus of the authors' research program in the recent past (see Fig. 1). The system requires no moving parts, which decreases the vibration level and enhances reliability. Compression of the refrigerant working fluid is accomplished in this scheme via an ejector.

However, a key uncertainty, addressed in the current paper, is the design of the ejector to accommodate the two-phase flow, which occurs in many operating regimes of interest within the device.

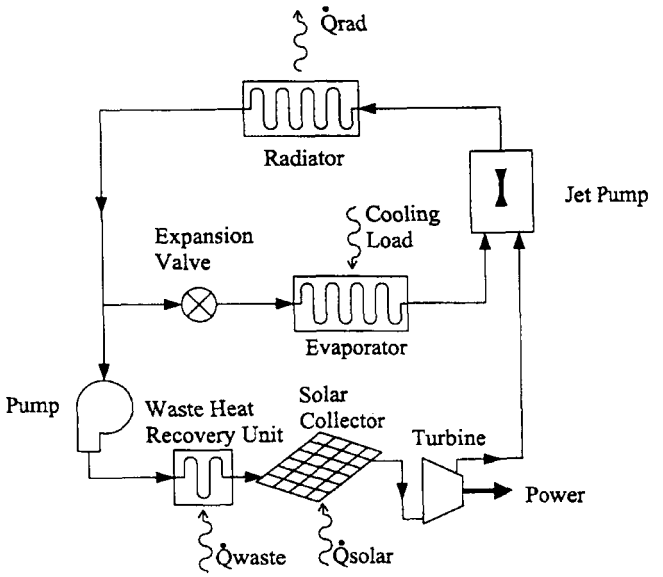

Figure 1. Schematic of the Solar Integrated Thermal Management and Power (SITMAP) cycle

Ejectors have been used in a wide variety of applications for over a century. Examples of applications for ejectors include vacuum pumps in the food industry, power stations, and in the chemical industry; ejector systems used in the aircraft industry for thrust augmentation; and steam-jet ejectors used in refrigeration. The ejector, shown schematically in Fig. 2, has the advantages of simplicity, no moving parts, low cost, and reliability. Other advantages of the ejector are decreases in both vibration and weight.

Literature dealing with ejectors is abundant, especially when dealing with single-phase flow. Single-phase ejectors exhibit a wide range of fluid phenomena and have historically incorporated the use of empirical methods in their design. However, for the case of two-phase flow in ejectors, there is little information readily available. More information about two-phase ejectors can be found in the works of Sherif et al. [1]. More research is needed in this area to be able to understand and design the ejector component, which would enable the potential mass savings of the SITMAP system.

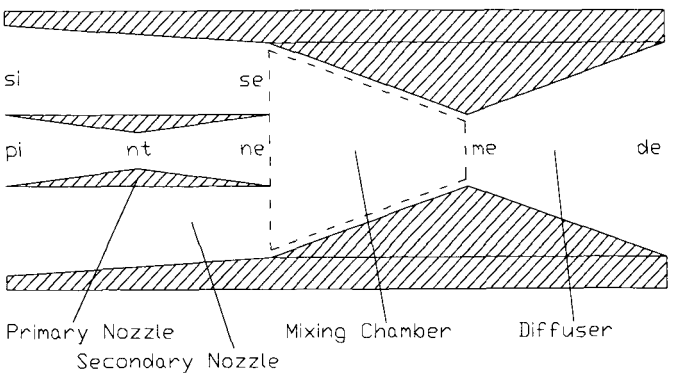

Figure 2. Schematic of ejector (non-constant area mixing)

The work to be presented in this paper is based on research conducted by Nord et al. [2], Freudenberg et al. [3], and Kandil et al. [4]. Nord et al. [2] developed the combined power and thermal management cycle for onboard spacecraft applications referred to above (i.e. SITMAP cycle). This is essentially an integrated vapor compression cycle and a Rankine cycle with the compression device being an ejector instead of the regular compressor. The power subsystem is a Rankine cycle, which drives the system. The ejector acts as the joining device between the thermal and power subsystems, by mixing the high-pressure flow from the power subsystem with the low-pressure flow from the refrigeration subsystem providing a pressure increase in the latter. Nord et al. [2] used Refrigerant 134-a as the working fluid in their analysis. The mechanical power produced by the turbine can be used to drive the mechanical pump as well as other onboard applications. This allows a system operating on the SITMAP cycle to be solely driven by solar thermal input.

Examples of work relevant to the SITMAP investigation include Bredikhin et al. [5], Cunningham and Dopkin [6], Cunningham [7], Elger et al. [8], Fabri and Paulon [9], Fabri and Siestrunk [10], Fairuzov and Bredikhin [11], Holladay and Hunt [12], Holmes et al. [13], Jiao et al. [14], Lear et al. [15], Marini et al. [16], Neve [17]and Sherif et al.

[1]. Literature dealing with thermally actuated cooling systems includes those by Kakabaev and Davletov [18], Chen [19], Lansing and Chai [20], and Chai and Lansing [21]. Many systems dealing with power and thermal management have been proposed for which the System Mass Ratio (SMR) analysis developed by Freudenberg et al [3] can be used, including absorption cooling systems and solar-powered vapor jet refrigeration systems. Examples of those systems are found in the works of Abrahamsson et al. [22], Alefeld and Radermacher [23], Anderson [24], Chai and Lansing [21], Chen [19], and Lansing and Chai [20].

This paper deals with an experimental investigation of a novel active thermal management system that we have proposed for use in space due to its potential for low weight and high reliability. Accordingly, this paper will present the design of an experimental facility for measuring the performance of constant-area ejectors with two-phase flow. Significant modeling has been performed in order to design this device, and the modeling approach will be described, along with the design choices in the construction of the facility. The purpose of the experimental investigation is two fold: to develop an experimental data set for two-phase ejectors (the key uncertainty in designing the proposed thermal management system) and to develop a proof-of-concept experiment for the thermal management system itself. The experimental results will be used to both calibrate the aforementioned model and also provide a high-quality design database of the global performance parameters of two-phase ejectors.

NOMENCLATURE

Latin Symbols

A	cross-sectional area, m^2
D	diameter
h	specific enthalpy, kJ/kg
m	mass, kg
$\dot{m}$	mass flow rate, kg/s
P	pressure, MPa
P_r	compression ratio
T	temperature, °C
V	velocity, m/s

Greek Symbols

ϕ	entrainment ratio, $\dot{m}_s / \dot{m}_p$

Subscripts

de	diffuser exit
me	mixing chamber exit
ne	primary nozzle exit
nt	primary nozzle throat
p	primary flow
pi	primary nozzle inlet
s	secondary flow
se	secondary flow exit
si	secondary flow inlet

EXPERIMENTAL DESIGN

The initial consideration in the experimental design process was to conceptually develop the best method of designing an ejector test rig that will be used to study the phenomena of two-phase flow mixing and compression. The primary design criterion established stated that the ejector primary and secondary nozzle inlet states were to be varied over a wide range of pressures, temperatures, and qualities in order to obtain a general database. The wide range of conditions is vital in thoroughly investigating the effects to two-phase flow. A second design requirement dealt with the ability to change the area ratios of the primary and secondary inlet and outlet nozzles. The computer program JetSit, written by Nord et al. [2], aided in the design of the ejector nozzles. JetSit, described below, is a computer program designed to model the SITMAP cycle and calculate the key ejector geometry parameters.

The first and most important design feature to accommodate was how to vary nozzle inlet states. Conceptually, some kind of loop must be designed to heat and cool the primary and secondary fluid flow. This heating and cooling process would necessarily

incorporate the use of one or more heat exchangers. In order to gain control of the pressure, a valve (e.g. adjustable throttling valve) would be needed. The working fluid must also be circulated through the loop; consequently, a pump would be needed. All of the components listed above are basic parts of a system operating on the SITMAP cycle. From this reasoning it was resolved that in order to gain relatively good control of the experimental apparatus, all components of that system would need to be incorporated. Since it was deemed advantageous to also obtain system-level data for the SITMAP cycle, the choice of ejector rig design was driven towards implementing that cycle directly.

Another important design consideration was the selection of a working fluid for the two-phase flow ejector test rig. The main criterion used in the fluid selection involved the temperature and pressure ranges where the fluid would be in the two-phase region. For safety reasons it was decided that the loop would be operated near ambient temperature and pressure. Information about individual fluids was found by examining their Material Safety Data Sheets (MSDS). Those sheets provide information that cover hazardous ingredients, health effects, handling details, fire and explosion hazard data, first-aid procedures, and critical fluid properties. An important critical fluid property found in the MSDS is the boiling point of a fluid. Since the fluid will be operated in the two-phase region, only fluids with a boiling point temperature slightly above ambient temperature were considered. Based on this information, R-141b was selected.

Experimental Setup

Once the working fluid was selected, the components were sized. Shown below in Fig. 3 is a schematic of the final layout of the experimental setup. It should be noted that both the boiler and evaporator have a controlled, measurable, and variable heat input. The heat input to the boiler can be varied from 0 to 5 kW, while that to the evaporator can be varied from 0 to 3.3 kW. This allows the ejector's primary and secondary inlets to be varied over a wide range of temperatures and/or qualities. It should also be noted that the pump design incorporates a bypass loop. This loop allows the pump to be operated at different speeds without changing the total mass flow rate through the rest of the piping system. Varying the pump speed allows the primary nozzle inlet pressure (P_{pi}) to be varied directly. The addition of the bypass loop also gives us the capability to vary the secondary nozzle inlet pressure (P_{si}) over a larger range. With this configuration, P_{pi} can be varied over a range of 0.5 MPa to 0.83 MPa, while P_{si} can be varied over the range of 0.15 MPa to 0.5 MPa. The condenser shown in Fig. 3 is a water-cooled condenser. The use of a condenser assures that the refrigerant at the pump inlet is always liquid. The charge or amount of refrigerant in the system is also adjustable. Different charge levels produce different mass flow rates and the pressures at all state points except during the phase change processes.

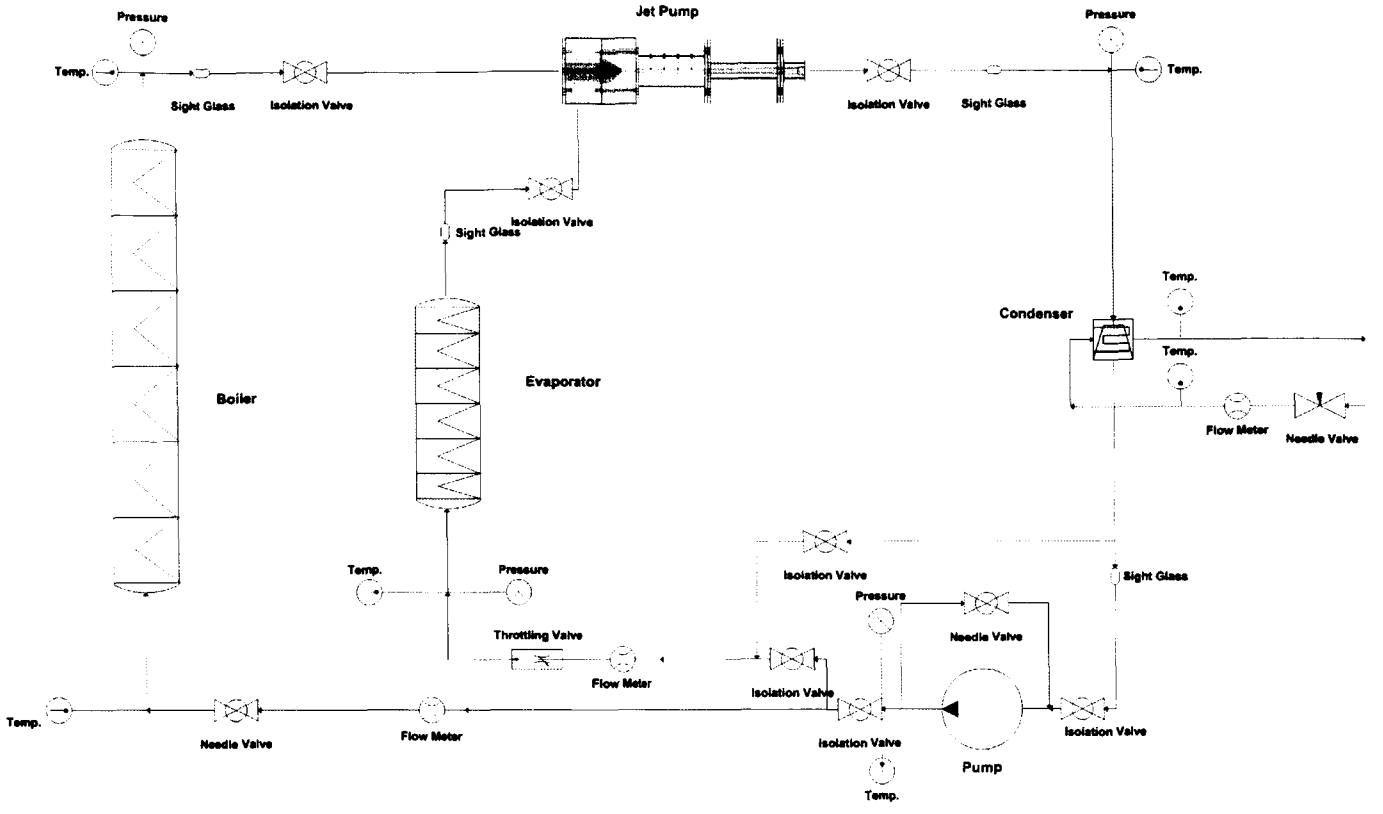

Figure 3. Schematic of the experimental testing apparatus

The arrangement of the aforementioned components used in conjunction with proper instrumentation allows the inlet conditions of the ejector to be varied over a wide range of conditions.

EJECTOR

Once the operating range of the testing apparatus was established, the ejector was designed. The ejector analysis is not included and the reader is referred to Nord et al. [2] for a detailed description of that part. Nord et al. [2] presented an iterative scheme that solves for the ejector exit state given the primary and secondary inlet states and the entrainment ratio. They then presented another iterative scheme to solve for all the other states in the SITMAP cycle given the output of the ejector analysis. The JetSit program referred to above was developed to efficiently perform the above ejector analysis and create performance graphs. JetSit's main functions are to calculate the ejector geometry and diffuser exit state and to use those results to calculate a solution to the SITMAP cycle. The program reads refrigerant properties from a data file, performs the necessary interpolations, uses the properties in the pump analysis schemes, and writes the results to a file. It should be noted that the JetSit code assumes constant-pressure mixing, whereas we use it for a guide for a constant-area mixing design. This is mentioned in more detail in the future work section. It should also be mentioned that JetSit is capable of analyzing ejector solutions for all flow regimes, including saturated flow.

The operating range of the testing apparatus was mapped into the inputs for the JetSit analysis. P_{si} was varied over the range of 0.15 MPa to 0.5MPa, while X_{si} was varied from 0.5 to 1.0. The entrainment ratio ϕ was varied from 0.2 to 2.0. The

primary inlet state was always in the superheated vapor region. Table 1 below shows some of the SITMAP inputs and their corresponding outputs. The ejector component outputs are the ejector compression ratio, the throat-to-exit area ratio of the primary nozzle, and the primary exit-to-secondary exit area ratio.

Table 1. Sample Inputs and Outputs of the Ejector Analyses

	SITMAP Inputs					SITMAP Outputs		
Cas	T_{pi}	P_{pi}	X_{si}	P_{si}	ϕ	P_r	A_{nt}/A	A_{ne}/A
1	13	.6	.7	.15	1.	1.65	.694	.222
2	13	.6	1	.1	1.	1.57	.694	.194
3	13	.6	.7	.1	.2	2.7	.694	1.223
4	13	.6	1	.1	.2	2.65	.694	1.067

Once the analysis has been performed over the range of specified conditions, the appropriate area ratios were determined.

Shown below in Fig. 4 is a schematic of the conceptual design of the ejector. The design is centered on the idea of a removable primary nozzle. In order to get multiple primary–to-secondary area ratios, multiple removable primary nozzles will need to be designed. The key to this design is to make it where the primary nozzle is easy to get to and easy to change. Making the nozzle easy to change will speed up the test phase.

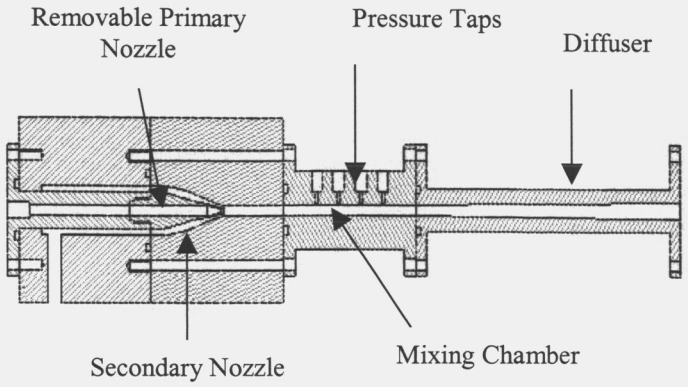

Figure 4. Ejector design

Once the basic ejector geometry has been fixed, the removable nozzle dimensions could be designed. This part of the design started by first fixing the mixing chamber diameter. Next the mixing chamber diameter was set equal to the outside diameter of the secondary nozzle, while the inside diameter of the secondary nozzle was set equal to the outside diameter of the primary nozzle. A schematic of this is shown in Figure 5. By using the above design geometry it is possible to achieve different area ratios A_{nt}/A_{ne} and A_{ne}/A_{se} by simply changing the primary nozzle. Using this technique, ten nozzles were designed to incrementally cover the desired range of area ratios.

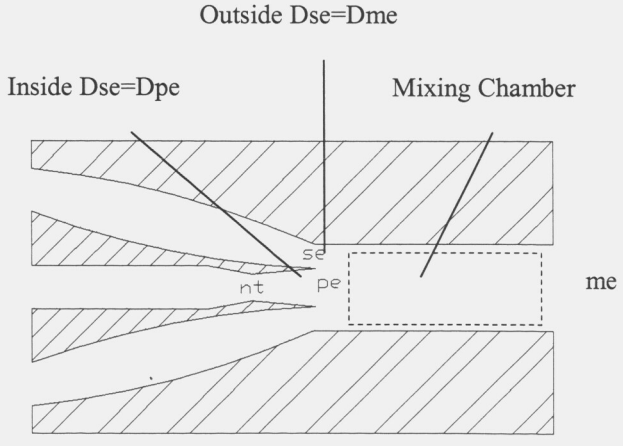

Figure 5. Constant-area ejector design

UNIVERSITY OF FLORIDA

EXPERIMENTAL PROCEDURE

An experimental procedure has been developed in order to systematically test the ejector over the desired range of conditions. The procedure involves a test plan using the variable heat inputs along with a range of valve settings to achieve specified pressures and temperatures. This allows the pump to be tested over the widest range of inlet conditions possible. The procedure is to be repeated for every nozzle, so that the geometrical effects of the primary nozzle expansion ratio and the primary-to-secondary area ratio may be studied. The data obtained will be reduced using a generalized equation of state, so that the results will have maximum generality. Thus it is expected that the data obtained in this program will be applicable with reasonable accuracy to two-phase ejectors operating with other working fluids.

SUMMARY

An experimental rig has been designed in order to test constant-area ejector performance over a range of primary and secondary inlet conditions, concentrating on operation in the two-phase regime. The design allows P_{pi} to vary from 0.5 MPa to 0.83 MPa while P_{si} can be varied over the rage of 0.15 MPa to 0.5 MPa. Since the heat input to both the primary and secondary flow is controlled, the fluid for both streams can be liquid, two-phase, or superheated vapor. In addition, several ejector geometry design variables may be adjusted, allowing for multiple ejector area ratios to be tested. All support structure and flow components have been acquired, and the test facility is in the final stages of assembly. The system has been designed to implement the SITMAP cycle, allowing a preliminary performance database to be developed upon testing. The flexibility of this experimental test rig will also allow a high-quality design database of the global performance parameters of two-phase ejectors to be obtained.

FUTURE WORK

The JetSit code will be modified from its current form in order to accommodate certain analytical needs. The first change involves matching code inputs with experimental inputs. Currently JetSit is a design-oriented code and will need to have an analysis mode added to it. The current design mode only takes the ejector inlet conditions as inputs and allows the ejector geometry to automatically adjust to its optimum design point. A new analysis mode will need to have the ejector geometry as well as the inlet state points as inputs. By having the geometry as an input a direct comparison between the theoretical and actual results for a given geometry can be made.

The second change that will need to be made involves the governing equations. Currently the JetSit code is based on a constant-pressure mixing ejector; whereas, in this experimental setup, the ejector is constant-area. The current form of the code was used only as a guide to get a range of viable area ratios. The main difference in the ejector analysis is found in the mixing chamber. In the case of constant-pressure mixing $P_{ne} = P_{se}$; this must be changed in order to account for the case where $P_{ne} \neq P_{se}$. Using a control volume approach and comparing the momentum equation for each case help realize the differences in the ejector analysis. The constant-pressure control volume as shown in Fig. 1 yields Equation (1) and the constant-area control volume shown in Figure 5 yields Equation (2). In analysis mode, the modified JetSit code will implement Equation (2) in the mixing section.

$$\left(P_{ne} - P_{se}\right)A_{ne} = -\dot{m}_p V_{ne} - \phi \dot{m}_p V_{se} + \left(1+\phi\right)\dot{m}_p V_{me} \quad (1)$$

$$\left(P_{ne} - P_{me}\right)A_{me} + \left(P_{se} - P_{ne}\right)A_{se} = -\dot{m}_p V_{ne} - \phi \dot{m}_p V_{se} + \left(1+\phi\right)\dot{m}_p V_{me} \quad (2)$$

A series of tests must also be conducted in order to characterize the experimental apparatus and to aid in the interpretation of the ejector performance data. The tests will be performed under certain operating conditions in order to get data in the specified regions. The results obtained from the tests will be used to validate the results from the ejector analysis. Shown below in Figs. 6 and 7 are examples of some graphical methods that will be used to compare the test results to the analytical model. A graph similar to Fig. 6 will be used to show the effects that varying the secondary inlet will have on the ejector pressure ratio for fixed ejector geometry, over a range of entrainment ratios.

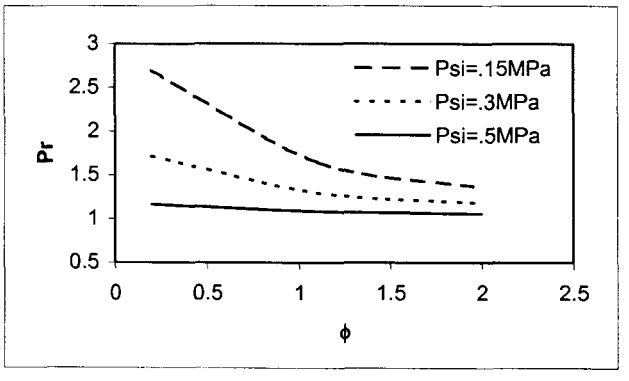

Figure 6. Performance curves of constant A_{nt}/A_{ne}, A_{ne}/A_{se}, T_{pi}, P_{pi}, and X_{si} for various design points

A graph similar to Fig. 7 will be used to show how the predicted ejector pressures ratio relates to the actual ejector pressure ratio. This will be used mainly for the validation of the model.

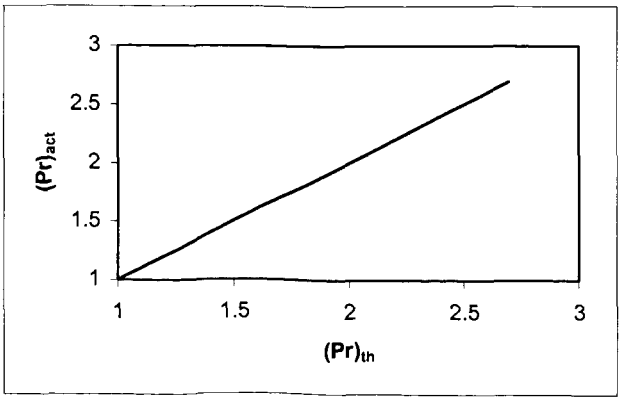

Figure 7. Predictions of performance relative to experimental findings

ACKNOWLEDGMENTS

This work was supported by NASA Glenn Research Center under grant number NRA-01-GRC-1 in the area of space power technology. Support from the Department of Mechanical and Aerospace Engineering at the University of Florida is also gratefully acknowledged.

REFERENCES

1. Sherif, S.A., Lear, W.E., Steadham, J.M., Hunt, P.L., and Holladay, J.B., "Analysis and Modeling of a Two-Phase Jet Pump of a Thermal Management System for Aerospace Applications," *International Journal of Mechanical Sciences*, Vol. 42, No. 2, February 2000, pp. 185-198.

2. Nord, J.W., Lear, W.E., and Sherif, S.A., "Design Analysis of a Heat-Driven Jet Pumped Cooling System for Space Thermal Management Applications," AIAA *Journal of Propulsion and Power*, Vol. 17, No. 3, pp. 566-570.

3. Freudenberg, K., Lear, W.E., Sherif, S.A., and Golliher, E.L., "Mass-Based Optimization of Thermal Management and Power Systems for Space Applications," AIAA *Journal of Propulsion and Power*, Vol. 18, No. 6, November-December 2002, pp. 1161-1169.

4. Kandil, S., Lear, W.E., and Sherif, S.A., "Performance of Jet-Pumped Cryogenic Refrigeration System," *40th AIAA Aerospace Sciences Meeting and Exhibit*, Reno, Nevada, January 14-17, 2002, AIAA Paper 2002-1031.

5. Bredikhin, V.V., Gorbenko, G.A., Nikonov, A.A., and Fairuzov, Y.V., "Mathematical Modeling of Thermo-Circulating Loops with

Jet Pumps," *Hydrodynamic Processes in Multi-Phase Working Fluid Energy Plants*, Kharkov Aviation Institute, Kharkov, Ukraine, pp. 3-10 (in Russian), 1990.

6. Cunningham, R.G. and Dopkin, R.J., "Jet Breakup and the Mixing Throat Lengths for the Liquid Jet Pump," ASME *Journal of Fluids Engineering*, Vol. 96, No. 3, pp. 216-226, 1974.

7. Cunningham, R.G., "Liquid Jet Pumps for Two-Phase Flows," ASME *Journal of Fluids Engineering*, Vol. 117, No. 2, pp. 309-316, 1995.

8. Elger, D.F., McLam, E.T., and Taylor, S.J., "A New Way to Represent Jet Pump Performance," ASME *Journal of Fluids Engineering*, Vol. 113, No. 3, pp. 439-444, 1991.

9. Fabri, J. and Paulon, J., "Theory and Experiments on Air-to-Air Supersonic Ejectors," NACA-TM-1410, September 1958.

10. Fabri, J. and Siestrunk, R., "Supersonic Air Ejectors," *Advances in Applied Mechanics*, Vol. V, H.L. Dryden and Th. von Karman (editors), Academic Press, New York, 1958, pp. 1-33.

11. Fairuzov, Y.V. and Bredikhin, V.V., "Two Phase Cooling System with a Jet Pump for Spacecraft," AIAA *Journal of Thermophysics and Heat Transfer*, Vol. 9, No. 2, April-June 1995, pp. 285-291.

12. Holladay, J.B. and Hunt, P.L., "Fabrication, Testing, and Analysis of a Flow Boiling Test Facility with Jet Pump and Enhanced Surface Capability," Research Proposal, NASA Marshall Space Flight Center, Thermal and Life Support Division, Huntsville, Alabama, 1996.

13. Holmes, H.R., Geopp, J., and Hewitt, H.W., "Development of the Lockheed Pumped Two Phase Thermal Bus," AIAA Paper 87-1626, June 1987.

14. Jiao, B., Blais, R.N., and Schmidt, Z., "Efficiency and Pressure Recovery in Hydraulic Jet Pumping of Two-Phase Gas/Liquid Mixtures," *SPE Production Engineering*, Vol. 5, No.4, 1990, pp. 361-364.

15. Lear, W.E., Sherif, S.A., Steadham, J.M., Hunt, P.L., and Holladay, J.B., "Design Considerations of Jet Pumps with Supersonic Two-Phase Flow and Shocks," *AIAA 37th Aerospace Sciences Meeting*, Reno, Nevada, January 11-14, AIAA Paper 99-0461, 1999.

16. Marini, M., Massardo, A., Satta, A., and Geraci, M., "Low Area Ratio Aircraft Fuel Jet-Pump Performance with and without Cavitation," ASME *Journal of Fluids Engineering*, Vol. 114, No. 4, 1992, pp. 626-631.

17. Neve, R.S., "Diffuser Performance in Two-Phase Jet Pump," *International Journal of Multiphase Flow*, Vol. 17, No. 2, pp. 267-272, 1991.

18. Kakabaev, A. and Davletov, A., "A Freon Ejector Solar Cooler," *Geliotekhnika*, Vol. 2, No. 5, September 1966, pp. 42-48.

19. Chen, L.T, "Solar Powered Vapor-Compressive Refrigeration System Using Ejector as the Thermal Compressors," *Proceedings of the National Science Council*, No. 10, Part 3, pp. 115-132, 1977.

20. Lansing, F.L. and Chai, V.W., "Performance of Solar-Powered Vapor-Jet Refrigeration Systems with Selected Working Fluids,"

DSN Progress Report 42-44, Jet Propulsion Laboratory, 1978, pp. 245-248.

21. Chai, V.W. and Lansing, F.L., "A Thermodynamic Analysis of a Solar-powered Jet Refrigeration System," DSN Progress Report 41-42, Jet Propulsion Laboratory, 1977, pp. 209-217.

22. Abrahamsson, K., Jernqvist, A., and Ally, G., "Thermodynamic Analysis of Absorption Heat Cycles," *Proc. of the International Absorption Heat Pump Conference*, New Orleans, Louisiana, AES-Vol. 31, ASME, 1994, pp. 375-383.

23. Alefeld, G. and Radermacher, R., *Heat Conversion Systems*, CRC Press, Boca Raton, Florida, 1994.

24. Anderson, H., "Assessment of Solar Powered Vapor Jet Air-conditioning System," *International Solar Energy Congress and Exposition (ISES),* Los Angeles, California, pp. 408, 1975.

UNIVERSITY OF FLORIDA

PROJECT TITLE: NEW PROPELLANTS AND CRYOFUELS

Task PI: Dr. Neil S. Sullivan, Department of Physics
Co-I: Dr. Jaha Hamida
NASA Contact: Bryan Palasezski, Glenn Research Center
External collaborator: V. Kokshenev, Univ. Federale de Minas Gerais, Brazil

PROJECT GOALS

The proposed research will investigate the stability and cryogenic properties of solid propellants that are critical to NASA's goal of realizing practical propellant designs for future spacecraft. We will determine the stability and thermal properties of a solid hydrogen-liquid helium stabilizer in a laboratory environment in order to design a practical propellant. In particular, we will explore methods of embedding atomic species and metallic nano-particulates in hydrogen matrices suspended in liquid helium. We will also measure the characteristic lifetimes and diffusion of atomic species in these candidate cryofuels.

The most promising large-scale advance in rocket propulsion is the use of atomic propellants; most notably atomic hydrogen stabilized in cryogenic environments, and metallized-gelled liquid hydrogen (MGH) or densified gelled hydrogen (DGH). The new propellants offer very significant improvements over classic liquid oxygen/hydrogen fuels because of two factors: (1) the high energy-release, and (ii) the density increase per unit energy release. These two changes can lead to significant reduced mission costs and increased payload to orbit weight ratios. An achievable 5-10% improvement in specific impulse for the atomic propellants or MGH fuels can result in a doubling or tripling of system payloads.

The high-energy atomic propellants must be stored in a stabilizing medium such as solid hydrogen to inhibit or delay their recombination into molecules. The goal of the proposed research is to determine the stability and thermal properties of the solid hydrogen-liquid helium stabilizer. Magnetic resonance techniques will be used to measure the thermal lifetimes and the diffusive motions of atomic species stored in solid hydrogen grains. The properties of metallic nano-particulates embedded in hydrogen matrices will also be studied and analyzed. Dynamic polarization techniques will be developed to enhance signal/noise ratios in order to be able to detect low concentrations of the introduced species. The required lifetimes for atomic hydrogen and other species can only be realized at low temperatures to avoid recombination of atoms before use as a fuel.

Goals for 2005

I. Manufacture and characterization of particulates. The goal is to test different techniques for producing the solid hydrogen matrices; slow adiabatic cooling of gas mixtures versus rapid injection of hydrogen gas into a pressurized cold helium gas cell. We propose to determine the particle size, diffusion constants and lifetimes of species introduced into matrices prepared by each method to determine optimum conditions for producing a stable cryogenic environment.

II. Introduction of metallic species into the hydrogen particles. We will test methods of introducing metals into the hydrogen matrices by using two different techniques: (i) radio-frequency (RF) discharge dissociation of molecular hydrogen in the cryogenic injection path, and (ii) evaporation of metallic atoms from hot filaments in the hydrogen/helium gas stream in the condensation stream. Magnetic resonance (MR) techniques are the most effective for studying the atomic species *in-situ* because the MR frequency of each species is unique and can be studied independently. By this means we can determine the stability and obtain information about the surroundings of different atomic species.

ACCOMPLISHMENTS

Samples of finely divided hydrogen and methane suspended in liquid helium have been made. Two different methods were tested: condensation from gas mixtures onto cold surface, and injection of H_2/He gas mixtures into cold helium gas

The thermal characteristics, notably the relaxation times and thermal diffusion were determined form NMR measurements of the relaxation times T_2 and T_1 that are directly related to the critical path of thermal stability and the internal diffusion of the host matrix.

Methane samples were explored and found to be significantly more favorable than hydrogen slush., The two cryogenic matrices were compared by measuring T_1 and T_2 on CH4/He slush and comparing with H2/He slush.

IMPORTANT CONCLUSIONS

Based on our experimental findings we conclude that solid H_2 is not suitable as a host matrix due to the strong surface interactions of ortho-hydrogen molecules with helium at the surface of the hydrogen granules. Since solid H_2 has a strong surface scattering due to its large electric quadrupole moment and its rotational motion that persists to low temperatures, we explored solid methane which has no quadrupole moment as a new matrix.
The results determined from the analysis for the microscopic correlation times τ leads to the following conclusions:

For hydrogen slush the NMR relaxation rate is consistent with scattering at grain boundaries and/or surface (due to large quadrupole moment Q of hydrogen).

For methane slush the NMR relaxation rate is consistent with the limiting factor in thermalization being internal diffusion as opposed to surface scattering.

In terms of a host matrix for atomic propellants methane is therefore a better host than hydrogen because the grains of methane are better isolated from the helium bath.

NEW RESULTS ON CH_4 / He SLUSH

From spin-spin relaxation times for freshly prepared methane-helium slush at 4.2K we found two different exponents which show the existence of two time scales in the system. As methane has a very complex ground state at low temperature we carried out our measurement on CH_4/He slush as the sample was aging with time. The new results show more than one time scales as the sample was aged.

UNIVERSITY OF FLORIDA

PUBLICATIONS AND PRESENTATIONS UNDER NASA GRANT

1. Marcin Matusiak, Jaha Hamida, Gary G. Ihas, Neil Sullivan, *NMR measurements in hydrogen/helium slush at 4.2 K*, Bull. Am Phys. Soc. **48**, 928 (2003).
2. M. Matusiak, J. A. Hamida, G. G. Ihas, N. S. Sullivan, *Measurements of the nuclear spin relaxation times for small grains of solid hydrogen suspended in liquid helium,* Presented at Quantum fluids and Solids International Symposium, 2003.
3. M. Matusiak, J. A. Hamida, G. G. Ihas and N. S. Sullivan, Journal of Low Temperature Physics (to be published).
4. J. A. Hamida and N. S. Sullivan, *Transport properties of bulk hydrogen and hydrogen-helium slush at 4 MHz using NMR measurements,* Bull. Am. Phys. Soc. **49**, 550 (2004).
5. J. A. Hamida and N. S. Sullivan, Nuclear spin relaxation times in hydrogen-helium and methane-helium slush at 4 MHz using pulse NMR, was presented at APS March Meeting 2005.
6. J. A. Hamida and N.S. Sullivan, *Nuclear Spin Relaxation Times for Methane-Helium "Slush" at 4 MHz using Pulsed NMR* submitted to the JLTP, Proceedings of the Internat. Low Temp Conference, Orlando, 2005.

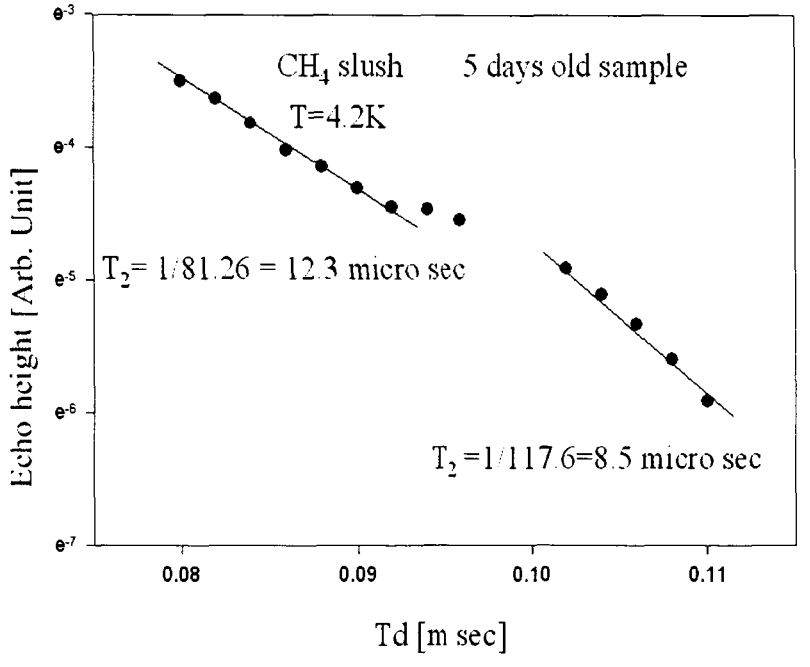

Figure1. Spin-spin relaxation times for methane-helium slush at 4.2K for 5days old sample. Two different exponents show existence of two time scales in the system.

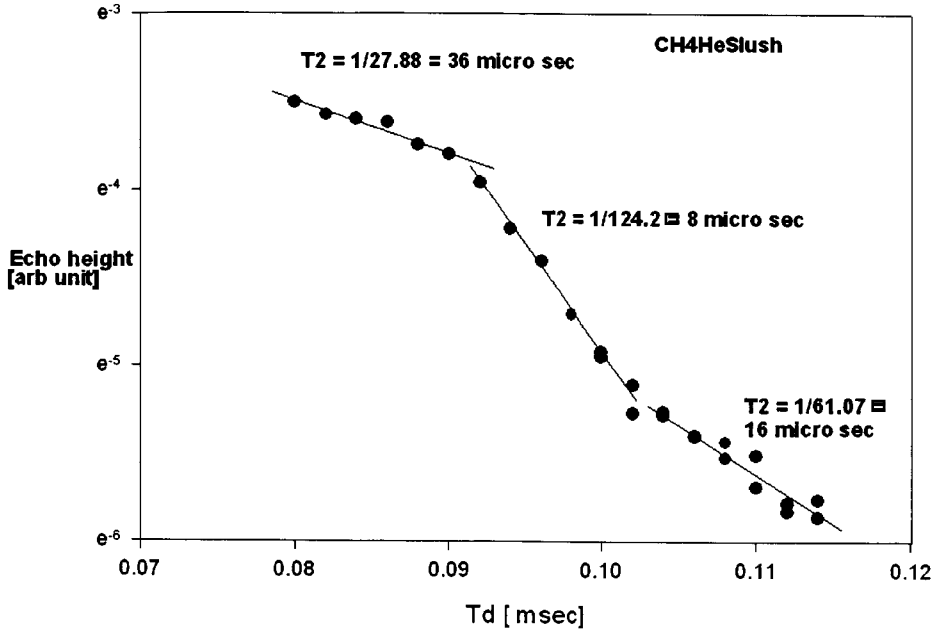

Figure2. Spin-spin relaxation times for methane-helium slush at 4.2K for 21days old sample. Three exponents show three different time scales in the system.

UNIVERSITY OF FLORIDA

PROJECT TITLE: ORTHO-PARA HYDROGEN RATIOMETRY

Task PI: Dr. Neil S. Sullivan, Department of Physics
Collaborator: Dawei Zhou

PROJECT GOALS

The research is devoted to developing efficient techniques to measure the ratio of the ortho and para hydrogen concentrations in gaseous samples. Special cells have been designed to measure the thermal conductivity of the gas mixtures at temperatures in the vicinity of 100 K. The thermal conductivity is very different for the two molecular species and this enables one to determine the ratio of ortho to para hydrogen very reliably. The effort has been focused on the need for a fast, high accuracy measurement using a simple compact cell. Tests of the design have been successful, and the last trimester of research was dedicated to optimizing an electronic readout package and demonstrating the sensitivity, stability, and speed of response of the ratiometer. We have also developed the basic design for a cryogen free ratiometer. We have also explored the development of high efficiency ortho-para converters.

Methods of measuring the ortho-para hydrogen ratio is very important for the manufacture, transport and storage of liquid hydrogen, and therefore critical for the space missions of NASA where liquid hydrogen fuels are employed. Because of the large heat of ortho-para conversion (670 J/g), incomplete conversion during liquefaction results in severe losses due to boil-off during storage and transport. Most manufacturers use a two-stage catalytic converter, at 77 K, and at 20.3 K in the liquefying process. At 300 K, the equilibrium concentration is 75% ortho, while at the boiling point (20.3 K), the equilibrium ortho concentration is 0.21%. The conversion at 77 K can produce 50% para-H_2, and the remaining conversion at 20.3 K consumes a significant fraction (~ 50%) of liquid hydrogen. From these considerations, one of the most important considerations in the production and storage of liquid hydrogen is the need for efficient cost-effective means of conversion from ortho to para hydrogen.[1] We are investigating a new conversion process using a highly efficient ortho-para hydrogen converter in the form of Cr_2O_3 powder as the active element. The oxide is contained in a continuous heat exchanger that allows the heat of conversion to be removed by the hydrogen gas flow.

ACCOMPLISHMENTS

1. We have modified the electronic readout circuit for the ortho-para ratiometer to optimize the speed of response of the thin-film circuit used to measure the thermal conductivity of the gas in the ortho-para hydrogen cell. The circuit diagram is given in Figure 1. The results of tests for the circuit to control current to maintain the resistance (temperature indicator) at a constant value is given in Table 1. The cell is shown in Figure 2.
2. We have changed one of the critical parameters of the ortho-para hydrogen ratiometer, namely the gap between the thin film sensor and the cold plate from 0.75 mm to 1.575 mm. The results for the new configuration are shown in Figure 3(c). The data is consistent with the change in geometry. The thermal conductivity of nitrogen gas has also been measured to provide a calibration test. The results show a similar pressure independent behavior for a wide range of pressure as seen in studies of hydrogen for similar current settings. The thermal conductivity data has shown a wide range of pressure independence up to 1.4 bar. This region of independence is consistent with

theory and indicates the design is successful in eliminating the effects of convection. The new results for the test are shown in Figure 3(a) and an expanded view is shown in Figure 3(b). We will also carry out measurements for different gases and different mixtures of ortho and para hydrogen.

3. Research has been initiated to test the efficiency of Cr_2O_3 as a catalytic agent for rapid ortho-para conversion. An ultra-fine chromic oxide powder (~1 micrometer diameter) is being considered for temperatures ranging from 4 to 25 K. (Figure 4)

Table 1: Bridge Controller Performance (Maintain Resistance as a Constant)

Operating Point:	6.9
Current Gain:	4.0
Cell Current:	70.01 mA
Cell Resistance:	10.05 Ω
Cell Power:	49.26 mW
Cell Current:	69.89 mA
Cell Resistance:	10.09 Ω
Cell Power:	49.29 mW
Cell Current:	70.13 mA
Cell Resistance:	10.01 Ω
Cell Power:	49.23 mW

Operating Point:	6.9
Current Gain:	8.0
Cell Current:	69.71 mA
Cell Resistance:	10.05 Ω
Cell Power:	48.84 mW
Cell Current:	69.39 mA
Cell Resistance:	10.09 Ω
Cell Power:	48.58 mW
Cell Current:	70.03 mA
Cell Resistance:	10.01 Ω
Cell Power:	49.09 mW

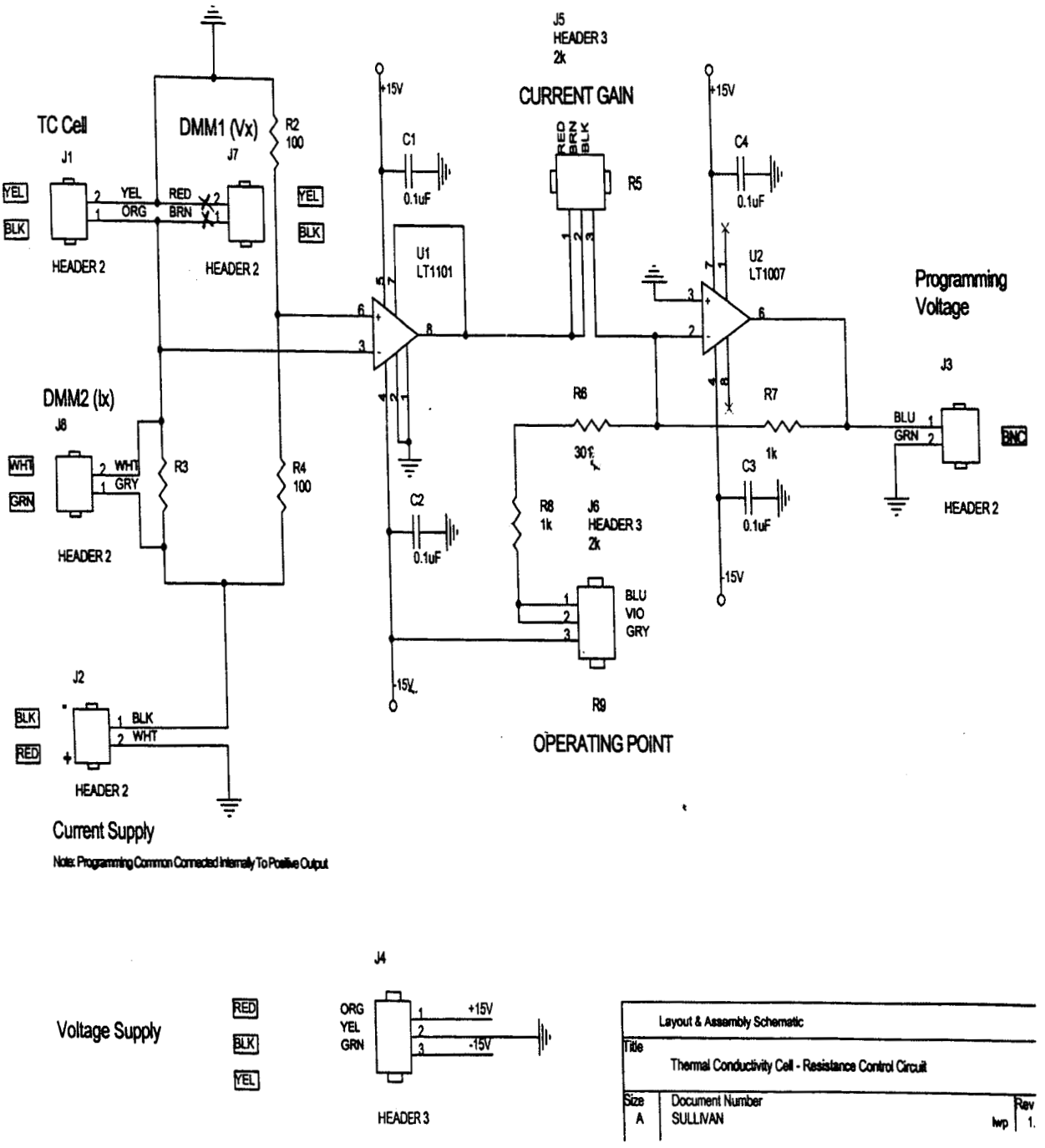

Figure 1: Schematic Circuit Diagram of Bridge Control for a Constant Resistance

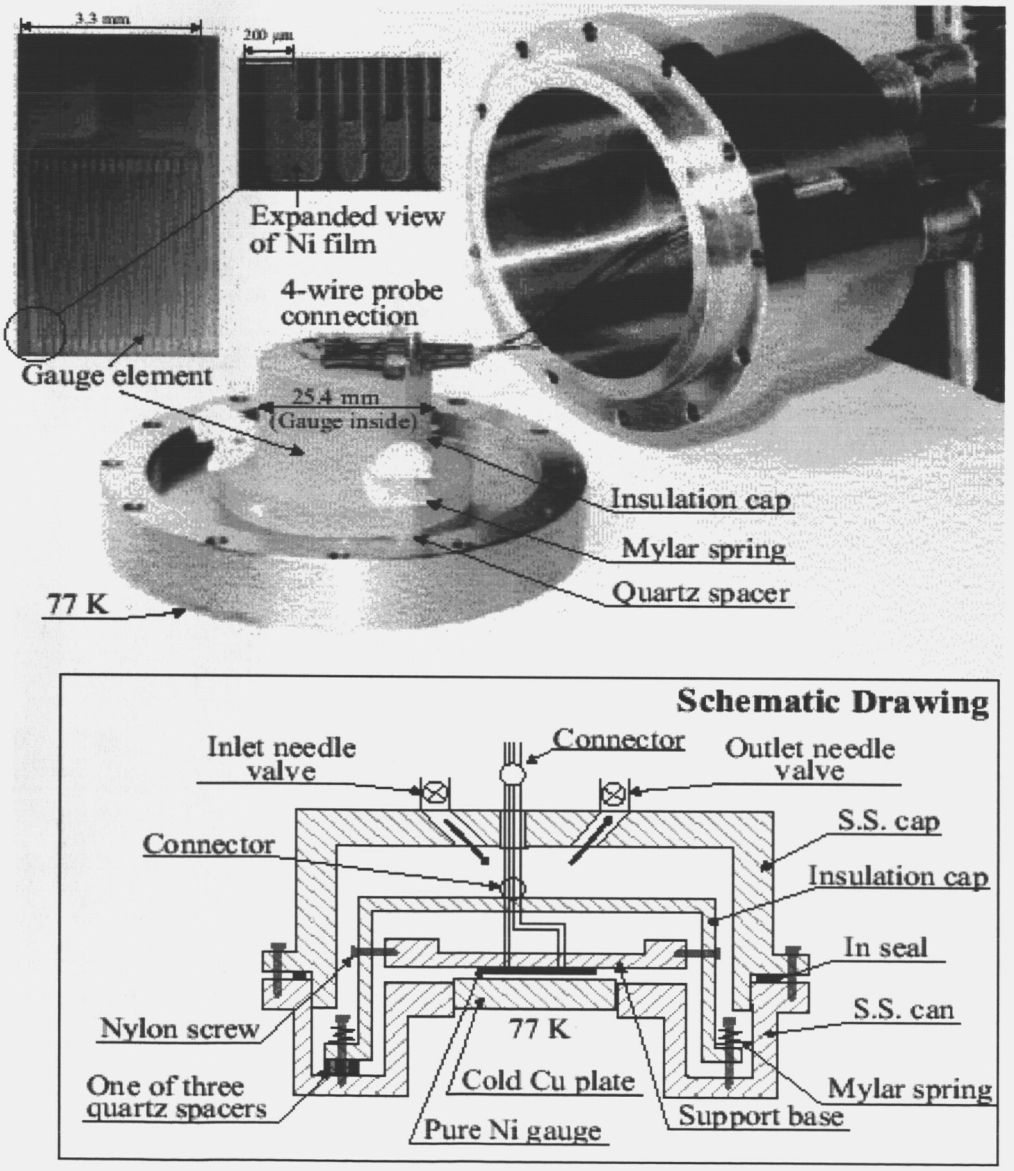

Figure 2. Ratiometer Design and Construction

Measurement by the Constructed Ratiometer

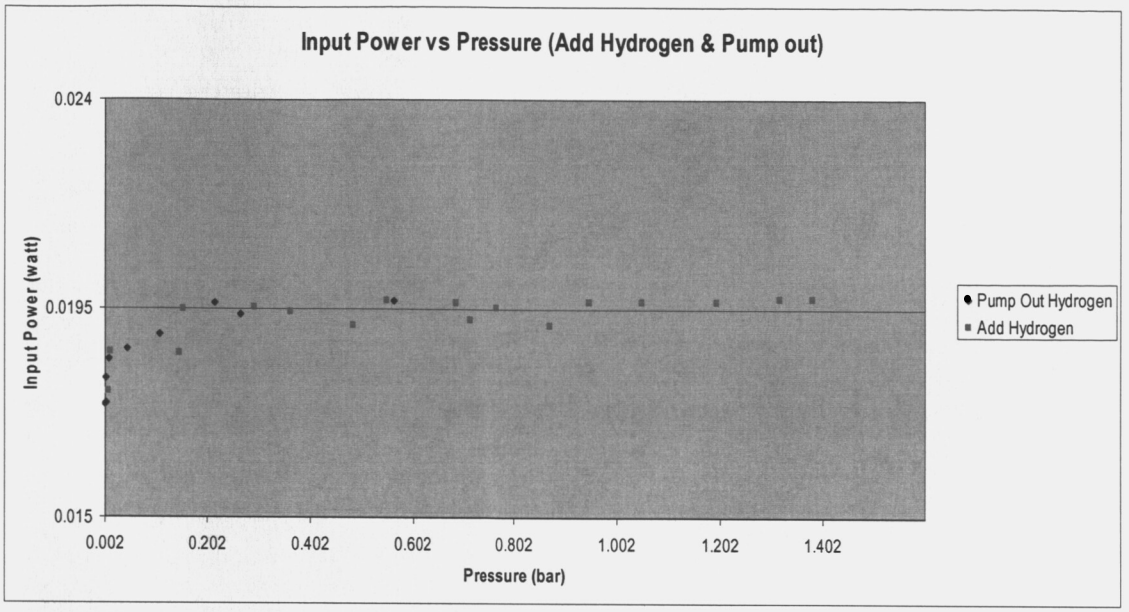

Figure 3(a)

Expanded View

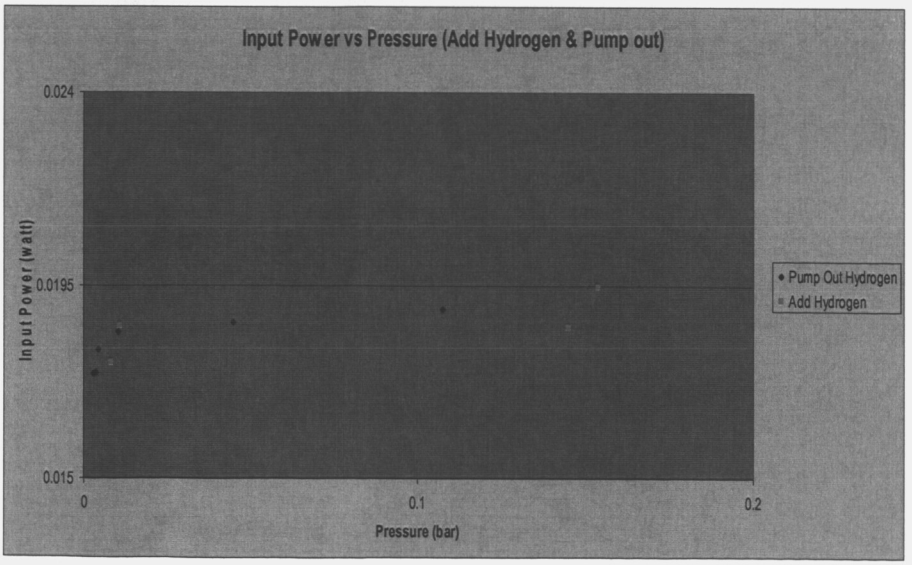

Figure 3(b)

UNIVERSITY OF FLORIDA

Hydrogen &Nitrogen Gas Measurement

(Gap between film and cold plate changed to 1.575 mm)

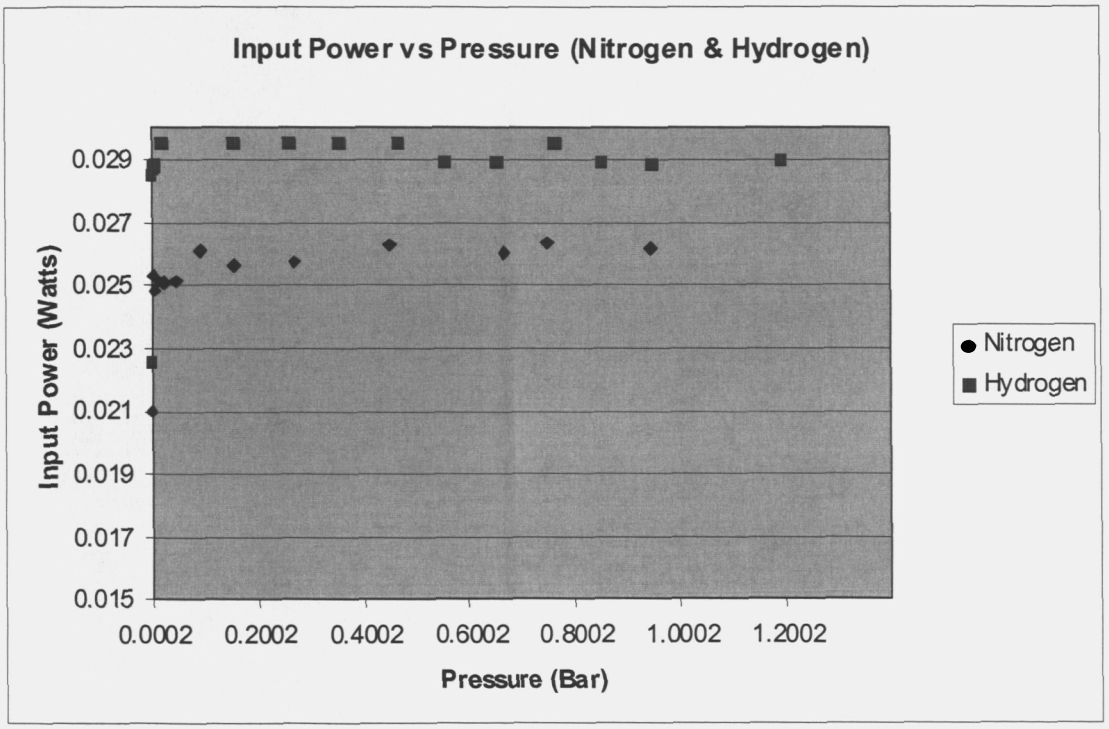

Figure 3(c)

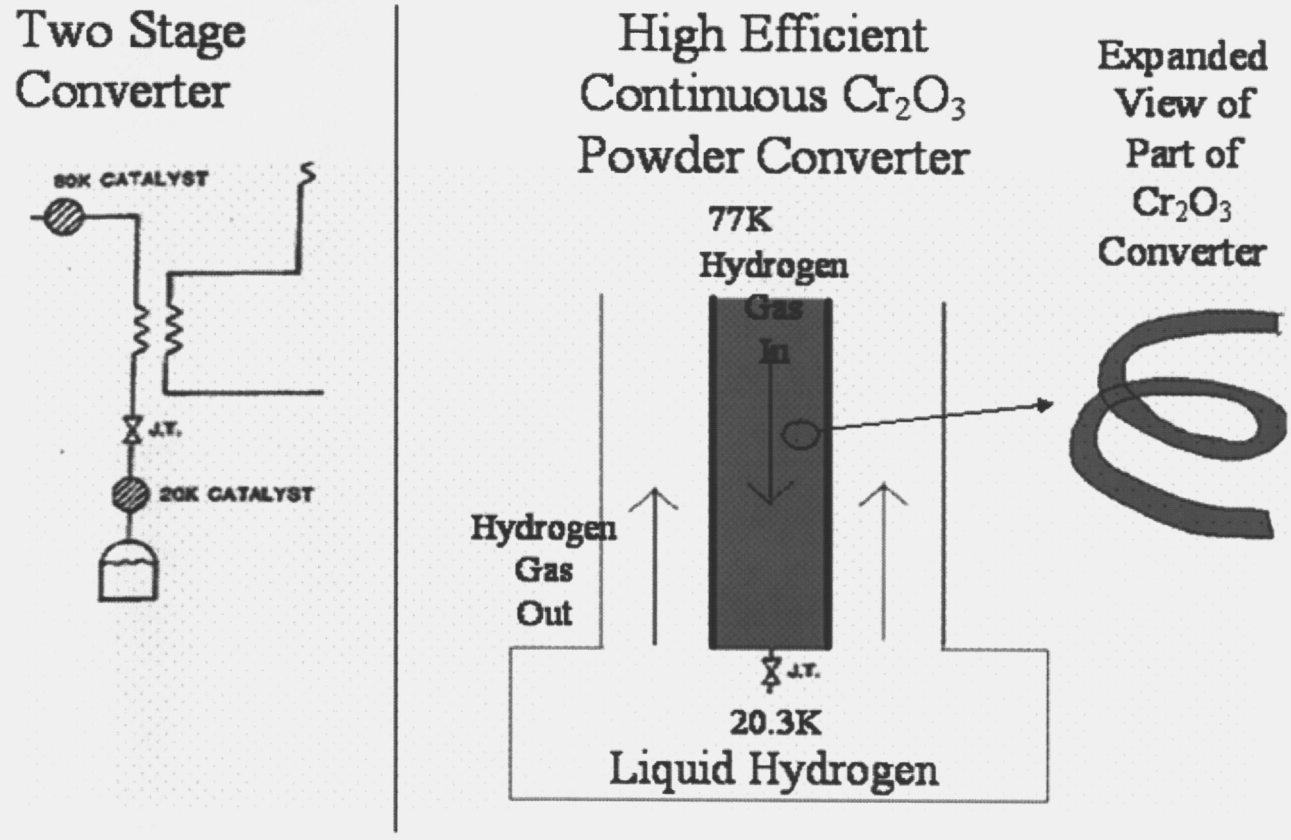

Figure 4. Cr_2O_3 as a catalytic agent for rapid ortho-para conversion

References

1. A. Farkas, *Orthohydrogen, parahydrogen and heavy hydroge*n, Cambridge University Press, Cambridge, UK, 1935.
2. I. F. Silvera, *Rev. Mod. Phys.* **52**, 393 (1980).
3. G. K. White, *Experimental Techniques in Low Temperature Physics*, Clarendon Press, Oxford, 1968, p. 47, 119.
4. T. M. Flynn, *Cryogenic Engineering, Marcel Dekker*, Inc., New York, 1977, p. 130.
5. N. S. Sullivan, D. Zhou and C. M. Edwards, *Cryogenics,* **30**, 734 (1990).
6. K.D. Williamson, Jr., F. J. Ederskuty, *Liquid Cryogens V1*, CRC Press Inc., 1983, p. 96 - 100.
7. E. R. Grilly, *Rev. Sci. Instr.* **24**, 72 (1953).
8. M. Devoret, N. S. Sullivan, D. Esteve and P. Deschamps, *Rev. Sci. Instr.* **51**, 1220 (1980).
9. N. V. Tsederberg, *Thermal Conductivity of Gases and Liquids*, Technology Press, Cambridge, Mass., 1965.
10. J. E. Jensen, R. B. Stewart and W. A. Tuttle, *Natl. Bur. Standards. Rept.* 8812 (1955).
11. J. O. Hirshfelder, C. F. Curtiss, and R.B. Bird, *Molecular Theory of Gases and Liquids*, Wiley, New York, 1954.
12. W. A. Wakeham, *J. Phys. E* **4**, 443 (1971).
13. A. B. Littlewood, *Gas Chromatography, Academic Press*, New York, 1962, Chap. 10.
14. D. Zhou, G. G. Ihas, and N. S. Sullivan, *Bull. Am Phys. Soc.*, **48**, 1277 (2003).
15. Vishay Measurements Group Inc., Rayleigh, NC.

Publications

1. D. Zhou, G.G. Ihas and N.S. Sullivan, Determination of Ortho-Para Ratio in Gaseous Hydrogen Mixtures, Journal of Low Temperature Physics, **134**, 401 (2004).
2. D. Zhou and N.S. Sullivan, Presentation at NASA Hydrogen Review Meeting, March 4, 2004.
3. D. Zhou and N. Sullivan, Ortho-*para hydrogen ratiometer design*, presented at Proceedings of the Internat. Low Temp. Physics Conference, Orlando, 2005.

UNIVERSITY OF FLORIDA

PROJECT TITLE: HIGH ENERGY DENSIFIED MATERIALS

Task PI: Gary G. Ihas, Department of Physics
Post Doctoral Associate: John T. Graham, Department of Physics

PROJECT GOALS

The major impetus in the recent surge in the study of solid hydrogen and in particular the study of chemical species isolated in solid hydrogen has been the possible use of the material as rocket fuel. The incentive to this was the suggestion that metal atoms could be used as performance improving additives to the current state of the art liquid oxygen/ liquid hydrogen propellant system. The major point of interest is the specific impulse I_{sp} of the propellant system, which is a measure of the momentum transferred to the vehicle per mass of the working fluid expelled from the rocket engine, and is proportional to the mean velocity of the exhaust. The specific impulse is proportional to the specific enthalpy of the chemical reaction occurring in the engine, and so can be changed by introducing dopants. Table 1 shows the theoretical specific impulses and their percentage change for 5% mole concentration of atoms in solid hydrogen propellants compared with the current liquid hydrogen system, reprinted from Fajardo et al (1).

Table 1: Theoretical specific impulses of atom doped solid hydrogen propellants

Additive	I_{sp}	% improvement
None	389	-
H	407	+5
Li	401	+3
Be	451	+16
B	470	+21
C	469	+21
N	414	+6
O	411	+6
F	398	+2
Na	373	-4
Mg	398	+2
Al	425	+9
Si	432	+11
Ti	404	+4

Clearly the systems of interest in this study are beryllium, boron, carbon, silicon and possibly aluminum. The major point of note is that this is a theoretical study and assumes that there is no interaction between the atomic species and the solid hydrogen. Several questions are raised by this study. First, can the atomic species of interest be actually produced and entrapped in solid hydrogen at 2 or 4 K? Second, to what degree does the atom interact with the solid hydrogen, and are molecular species produced?

These questions may be answered by reviewing the open academic literature considering either studies of species in solid hydrogen or matrix isolation studies in noble gas matrices where the matrix is doped with a small amount of hydrogen.

In our earlier reports we reviewed the open academic literature considering the entrapment of either boron or carbon in hydrogen matrices or in noble gas matrices where the matrix is doped with a small amount of hydrogen. In review, although it appears that both boron and carbon vaporizing species interact with hydrogen, boron vaporizes as an atomic or dimeric species whereas carbon vaporizes in a plethora of carbon chain species the nature of which is being studied extensively by many research groups using matrix isolation. See, for example, studies by Larson (2) and Meirs (3), including detailed studies using hydrogen as the isolating matrix.

ACCOMPLISHMENTS

Boron in Solid Hydrogen

Boron and carbon are considered of interest due to the high percentage improvements in the I_{sp}. Our first candidate for study was be boron. It is well known that boron vaporizes as boron atoms and the dimeric species B_2 (4), and it is believed that boron atoms may be easily trapped in solid hydrogen. A theoretical study (5) indicated that the reaction path

$$B + H_2 \rightarrow BH_2$$

was unlikely to occur. To date, two major studies have vaporized boron into solid hydrogen. Fajardo et. al. (6) used ultraviolet \ visible spectroscopy to study the process and noted that although the resulting spectra were similar to those observed in rare gas matrices, there were significant frequency shifts. In the field of matrix isolation spectroscopy, major frequency shifts between matrices can sometimes be an indicator of the isolated species interacting with the surrounding matrix. The second study vaporizing boron into solid hydrogen was done by Weltner et. al . (7) using electron spin resonance (esr) as the identifying technique. The sole species identified was boron tetrahyride (BH_4); no boron atoms were observed. The esr spectrum of boron atoms is complex but very distinctive and has been the subject of much study (8,9).

There is clearly a conflict in the open literature, with one study indicating the possibility of boron atoms, and the other study concluding that all of the boron reacts with hydrogen to form BH_4. Supplementary clues are obtained by the studies of Andrews et al (10,11). In a detailed study Andrews and Tague (10) vaporized boron in argon matrices doped with amounts of hydrogen and found that a plethora of boron hydride species were formed. Increasing the hydrogen content and trapping in neon resulted in the production of the species BH_4 and BH_4^- (11); all of these species were characterized using infrared spectroscopy. The literature evidence suggests that boron readily reacts with hydrogen to possibly form a variety of species but predominately hydrogen boron tetrahydride. In addition, boron readily reacts with trace impurities in the matrix gas (see for example discussion in ref (10)). This is known and has been studied extensively, but may increase the difficulty in interpreting results if ignored.

Carbon in Solid Hydrogen

Studies of the vaporization of graphite and the subsequent entrapment of the vapor in hydrogen have followed the pattern of the noble gas matrices. Van Zee et. al. (12) vaporized graphite and

using esr spectroscopy identified the species C_4 in solid hydrogen, whereas by using deuterium obtained spectra for C_4, C_6, C_8 and C_{10} . Using infrared spectroscopy Shida et. al. (13) identified the species C_3 C_5 C_9 and other clusters. It is interesting to note that no hydrocarbon species were observed. Tam et. al. (14) vaporizing graphite into hydrogen matrices also observed the carbon species C_3 ,C_6 ,and C_9, as well as the hydrocarbon species CH_4 and CH_3 . It was noted that the CH_4: C_3 ratio increased dramatically as the laser ablation energy increased. This is consistent with the mass spectrometric study by Kato et. al. (15) of the vaporization of graphite in the presence of hydrogen and deuterium gasses. The conclusion of this study was that hydrocarbon species originate mainly from the reaction of carbon species and the thermally decomposed hydrogen atoms produced by the intense vaporization pulses.
The major conclusion from the literature on carbon species entrapped in solid hydrogen is that there is a general consensus on which carbon species are isolated and that the infrared spectra are of a very high quality. This was the main reason that we chose to make our initial studies on the boron / hydrogen system.

Apparatus

In our previous reports we described the construction and initial testing of our cryostat. In summary, cool down of the polished aluminum support from room temperature to circa 4 K was achieved routinely in less than ten minutes. Figure (1) shows a cross sectional view of the lower section of the cryostat showing the positioning of the boron sample relative to the polished aluminum sample support and the access window for the laser. Figure (2) shows a typical experiment in progress. The cryostat (a) is mounted on a custom made optical bench, which enables consistent positioning of the cryostat relative to the external sampling port of the Bruker infrared spectrometer (b). The movable pumping station (c), consisting of a diffusion pump and a backing rotary pump, is connected to the cryostat via a flexible vacuum line. The computer console (d) runs the spectrometer and analyzing spectra. The panel (e) is the hydrogen handling and purification system. Liquid helium is transferred from the liquid helium dewar (f) via the flexible transfer line (g) to the cryostat; exhaust gas is collected by the flexible recovery line (h), which is connected to the permanent laboratory recovery system (i). The Nd:YAG laser (j) with steering optics have been temporarily moved aside. The movable pumping station with flexible vacuum line (c) and the flexible recovery line (h) are features that enable the rotation of the top section of the cryostat and the inner cold finger under cryogenic and high vacuum conditions
The spectrometer used is a Bruker IFS-113 with p.c. control, the laser used is a Nd:YAG pulsed q switched and frequency doubled, and is used under conditions known to vaporize the vast majority of materials.

Deposition of Solid Hydrogen at 4 K

To produce a sample for study, a solid hydrogen film was formed on the polished aluminum support by cooling the cryostat down to 4 K and then slowly bleeding hydrogen into the hydrogen inlet line using a needle valve. Figure (3) shows a typical infrared spectrum obtained after about twenty minutes deposition, without utilizing the purification system. The infrared spectrum exhibits the fundamental vibrations for carbon dioxide and monomeric water (16), in addition to weak features labeled (*) due to hydrocarbons. All three species are known to be trace impurities in many gasses including hydrogen, and carbon dioxide and water have been characterized in solid hydrogen (17,18). The bands assigned to carbon dioxide and water are particularly striking as those molecules are very strong infrared absorbers and are often used as

internal calibrants. Utilizing the cold trap in the purification apparatus removes all of these features apart from a very weak absorbance at about 2345 cm^{-1}, which is the strong fundamental for carbon dioxide.

Vaporization and Trapping of Boron in Solid Hydrogen at 4 K

As shown in figure (1) the sample of solid boron is mounted in the vacuum chamber in such a way that the plume of laser ablated material is mixed with the large excess of hydrogen before being deposited on the cold polished support. Typically a thin bed of solid hydrogen is laid down on the polished surface prior to commencement of laser ablation. Infrared spectra are acquired every ten minutes of laser ablation in order to observe band growth and to assist spectral assignment. Occasionally laser ablation lasts up to one hour but is usually twenty to thirty minutes in duration. A typical experiment lasts several hours with no noticeable deterioration in spectral quality or relative band intensity changes.
Figure (4) shows a typical early infrared spectrum produced after the deposition of boron vapor and hydrogen without purifying the hydrogen, as usual residual impurities water, carbon dioxide and hydrocarbons are observed. However, two new bands are observed in the region 2250 to 2000 cm^{-1} that are within the B-H stretching region. The feature at about 2017 cm^{-1} is identified as a hydrolysis species such as HOBO. Later experiments exhibit spectra typical of figure (5) in which the feature at 2017 cm^{-1} is absent but a feature at about 474 cm^{-1} consistent with the species HBO is observed. In all of the experiments involving boron, a sharp band at 2138 cm^{-1} is observed. When this band is strong a feature at 1305 cm^{-1} appears to be growing with it. Purifying the hydrogen prior to deposition eliminates the infrared absorptions due to water and virtually eliminates the feature at 2345 cm^{-1} assignable to the strong fundamental of carbon dioxide. However, the features at 2138 and 1305 cm^{-1} are still produced.

We tentatively assign the infrared absorption at 2138 cm^{-1} to the chemical species BH_4 in addition to the feature at 1305 cm^{-1}. Andrews and Wang (11) assign four infrared absorptions to BH_4 in neon. However, it is believed they have a distorted tetrahedral system consisting of two short and two long B-H bonds with the bond angle between the two long B-H bonds a mere 46.7 degrees. This structure is consistent with the structure proposed by Weltner et. al. (7) who characterized BH_4 in hydrogen at 2K. We are proposing that BH_4 in hydrogen at 4K is more like the classic tetrahedral with all four B-H bonds essentially equivalent. It is known that solid hydrogen at 4K is a lot softer than the same solid at 2 K, which would enable the species to relax to the tetrahedral we are postulating. The difference in softness between 2 and 4K is one of the reasons that the majority of researchers operate at 2 K. Clearly further work is required to clarify the situation.

Vaporization and Trapping of Carbon in Solid Hydrogen at 4 K

A small chunk of high purity graphite was mounted in our sample chamber in a similar manner to that of boron, was ablated using the Nd:YAG laser, and the resulting vapor isolated in a hydrogen matrix. Figure (6) shows a typical infrared spectrum after about 30 minutes of vaporization / deposition. By comparison with the earlier literature studies, we can readily identify the carbon species C_3 ,C_6 ,C_5 ,and C_9 , as well as a very weak absorbtion assignable to the species CH_3 . It is important to note that we did not observe the species CH_4 which has been extensively studied in hydrogen matrices (19) and was observed by Tam et al (14). Of interest are the two weak features marked * and may be the species $C(H_2)$. This species has been the

subject of extensive interest and questions have been recently raised (20) concerning how atomic carbon interacts with molecular hydrogen, whether it forms an adduct species $C(H_2)$, or if it goes all the way and inserts into the hydrogen molecule to form the molecular species CH_2. The positions and relative intensities of the two infrared bands will help to tackle this question as a dipole induced by the carbon atom in the hydrogen molecule may induce infrared activity.

Continuous Flow Liquid Helium Cryostat

We have constructed a 'bare bones' continuous flow liquid helium cryostat designed for infrared studies of solid hydrogen and isolated molecular species at either 2 or 4 K. A detailed description of the cell construction and testing has been published (21). The use of a heater we installed will enable studies up-to about 6 K, which opens up the possibility of diffusion and stability studies. To date, all of our studies have been at 4K which is a testament to the skill and expertise of the Physics Department Machine Shop and Cryogenic Services in the construction and design of the cell.

We have been able to routinely trap high temperature chemical species in solid hydrogen at 4 K using this apparatus and produce stable matrices for study at leisure. The majority of researchers usually operate at 2 K when trapping species in hydrogen due to the fickle nature of solid hydrogen. A temperature of 2 K is obtained by pumping on the liquid helium coolant with a roughing vacuum pump resulting in evaporative cooling, but at the expense of higher liquid helium consumption.

In this project we have demonstrated the vaporization of both boron and carbon and trapped the resulting vapors in solid hydrogen as initially proposed by us. In addition, preliminary analysis of the infrared spectra, indicate that molecular species such as boron hydrides and carbon chains or clusters are formed rather than solely atomic species.

This work was briefly mentioned in an article in *Cold Facts*, the magazine of the Cryogenic Society of America Inc., authored by Van Sciver (22). In the article our aims, goals, and techniques were gratefully mentioned. However, the article claimed that our work was the first to embed carbon and boron in solid hydrogen. This is not the case. Many groups have preceded our work (Weltner, Fajardo, Andrews, Momose, and Shida to list a few), and we have benefited greatly from them.

Further Studies

The theoretical specific impulses calculated by Carrick (23) and quoted by Fajardo et al (1) assumed the ability to produce solely atomic species at a concentration of 5% in solid hydrogen. This would result in a significant improvement in the specific impulse of the rocket. We have demonstrated that the vaporization of either boron or carbon results in the generation of a plethora of molecular species, which is entirely consistent with previous studies of the systems in noble gas matrices and mass spectrometric studies.

In order to accurately access the validity of high energy densified fuels based on impurity doped solid hydrogen as the new generation of rocket fuels, calculations need to be made on solid hydrogen doped with molecular species such as C_3 or BH_4, rather than the imagined atomic species.

The next step in this work would be to improve the quality of the infrared spectra and to confirm the spectral assignments. The use of isotopes such as ^{12}C, ^{13}C, ^{10}B, ^{11}B, ^{1}H, and ^{2}H (D) is one of the most powerful tools available to the matrix isolationist for spectral identification. Further analysis of the data will be needed to order to attempt to quantify the relative concentrations of the chemical species, in particular the carbon system. The possible presence of $C(H_2)$ in the carbon system offers the exciting possibility of being able to monitor the interaction of an atomic species with hydrogen, whether it is with the bulk hydrogen or a single hydrogen molecule.

The use of infrared spectroscopy to monitor the generation of species produced by the reaction of boron atoms and dimmers with trace impurities such as water and carbon dioxide (not just hydrogen) is of immense value as impurities will always be present and they should not be ignored.

We are at present unable to pursue any of this exciting research, as our funding was not renewed. We are aware that this research offers few if any immediate applications or financial savings to NASA, but it is much more difficult to dismiss the long term applications of such exciting research results.

ACKNOWLEDGEMENTS

This Work was supported by NASA Glenn Research Center under the contract (NAG3-2930). We would also like to thank the Department of Physics Machine Shop for their expertise in the design and construction of the cryostat, and Cryogenic Services at the Department of Physics, in particular Greg Labbe, for its extensive assistance in the field of cryogenic engineering. The UF Department of Chemistry is also acknowledged for use of the infrared spectrometer. In addition, we would like to thank the following students Jenn Sirak (REU Student – Rutgers), Nathan Heston (Graduate Student), Erick Hernandez (Undergraduate Student), and Mario Pardon (Undergraduate Student) for assistance.

References

1. M. E. Fajardo, S. Tam, T. L. Thompson, M. E. Cordonnier, Chem. Phys. **1994** 189 351 and references therein.

2. C. Larson, W. Harper, J. Presilla-Marquez, Matrix Isolation of Boron and Carbon Vapor. (2000), 15(Pt. 1, High Temperature Materials Chemistry, Part 1), 349-352. AN 2001:340042

3. J. P Maier, J. Phys. Chem. A **1998**, 102(20), 3462

4. See for example L. B. Knight, B. W. Gregory, S. T. Cobranchi, D. Feller, E. R. Davidson. J. Am. Chem. Soc. **1987** 109 3521

5. M. H. Alexander. J. Chem. Phys. **1993** 99 6014

6. S. Tam, M. Macler, M. E. DeRose, M. E. Fajardo. J. Chem. Phys. **2000** 113 9067, M. E. Fajardo, S. Tam J. Chem. Phys. **1998** 108 4237

7 R. J. Van Zee, A. P. Williams, W. Weltner Jr. J. Chem. Phys. **1997**, 107 4756

8 A detailed description of the esr of boron atoms is given in :-W. Weltner Jr. Magnetic Atoms and Molecules Publ Dover pub New York 1989

9 T Kiljunen, J. Eloranta, J. Ahokas, H. Kunttu, J. Chem. Phys. **2001**, 114(16), 7144

10 T. J. Tague Jr., L. Andrews J. Am. Chem. Soc. **1994**, 116, 4970

11 L. Andrews, X. Wang. J. Am. Chem. Soc. **2002** 124 7280

12 R. J. Van Zee, S. Li, W. Weltner Jr. J. Phys. Chem. **1993** 97 9087

13 M. Miki, T. Wakabayashi, T. Momose, T. Shida. J. Phys. Chem. **1996** 100 12135

14 S. Tam, M. Macler, M. E. Fajardo. J. Chem. Phys **1997** 106 8955

15 Y. Kato T. Wakabayashi, T. Momose, Chem. Phys. Lett. **2004** 386 279

16 See for example K. Nakamoto Infrared and raman of inorganic and coordination compounds Publ. J. Wiley New York 1997

17 S. Tam M. E. Fajardo. Low Temp. Phys. **2000** 26 653

18 M. E. Fajardo, S. Tam, M. E. DeRose J. Mol. Struct. **2004** 695 111

19 The sharpness and quality of the infrared spectra of methane isolated in hydrogen matrices is remarkable and the observation of rotational fine structure offers the ability for detailed analysis see for example a) T. Momose, T. Shida Bull. Chem. Soc. Jpn. **1998** 71 1 b) L. Li, J. T. Graham, W. Weltner Jr. J. Phys. Chem. **2001** 105 11018 c) T. Momose. H. Hoshina, M. Fushitani, H. Katsuki, Vibrational Spectroscopy **2004** 34 95 d) S. Tam, M. E. Fajardo, H. Katsuki, H. Hoshina, T Wakabayashi, T. Momose, J. Chem. Phys. Phys. **1999** 111 4191 e) T. Momose, M. Miki, T. Wakabayashi. T. Shida, M. Chan, S. S. Lee, T. Oka J. Chem. Phys. **1997** 107 7707 f) Y. J. Wu, X. Yang, Y. P. Lee, J. Chem. Phys. **2004** 120 1168

20 M. Vala, J. Szczepanski personal communication

21 J. T. Graham, G. G. Ihas J. Low Temp. Phys. **2005** 138(3/4) 923

22 S. Van Sciver Cold Facts Summer **2004** 20(3) p6

23 P. G. Carrick Specific Impulse Calculations of High Energy Density Solid Cryogenic Rocket Propellants 1: Atoms in Solid Hydrogen NTIS Report **1993** (PL-TR-93-3014 Order No. AD-A263208

Figure (1):- Cross Sectional View of the Cryostat

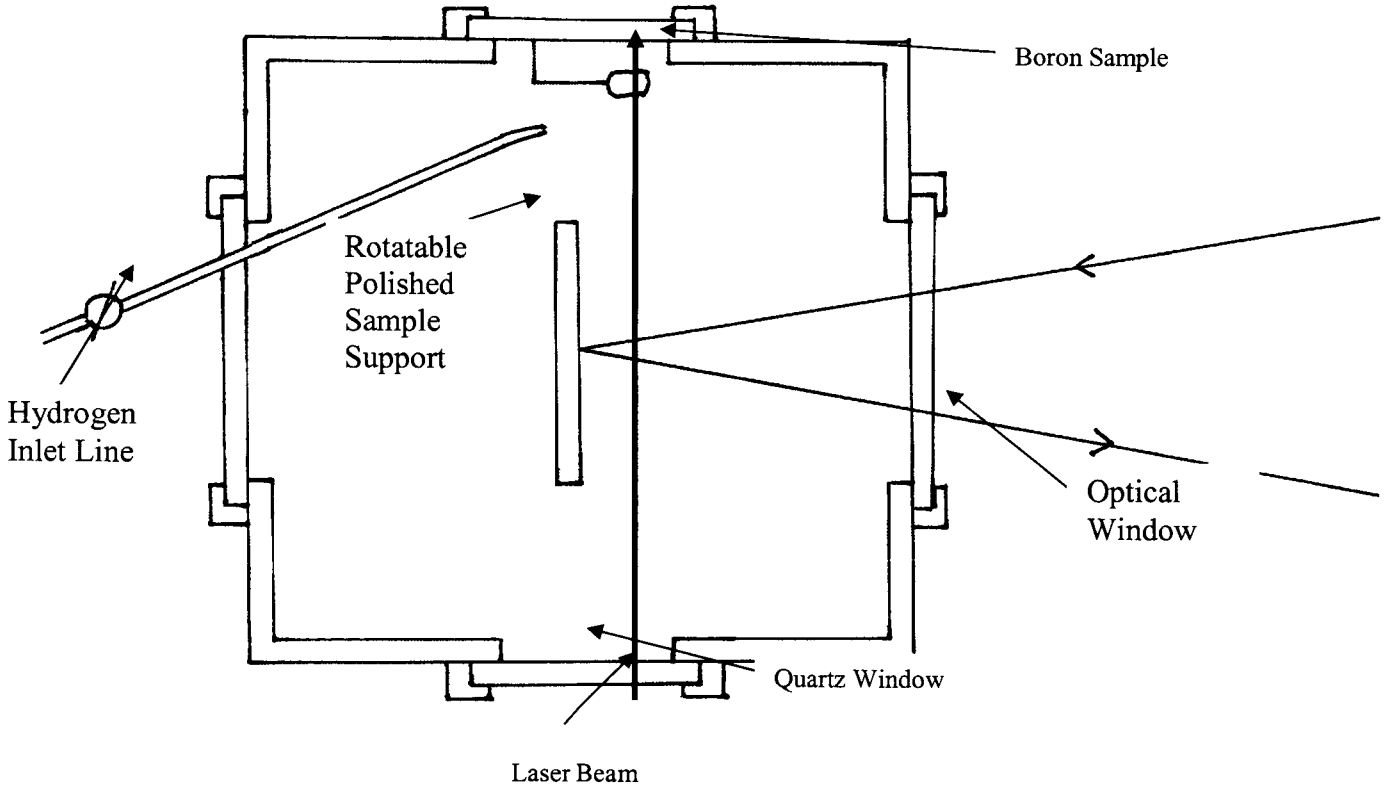

Figure (2):-Typical Experimental Setup (See text for explaination of symbols)

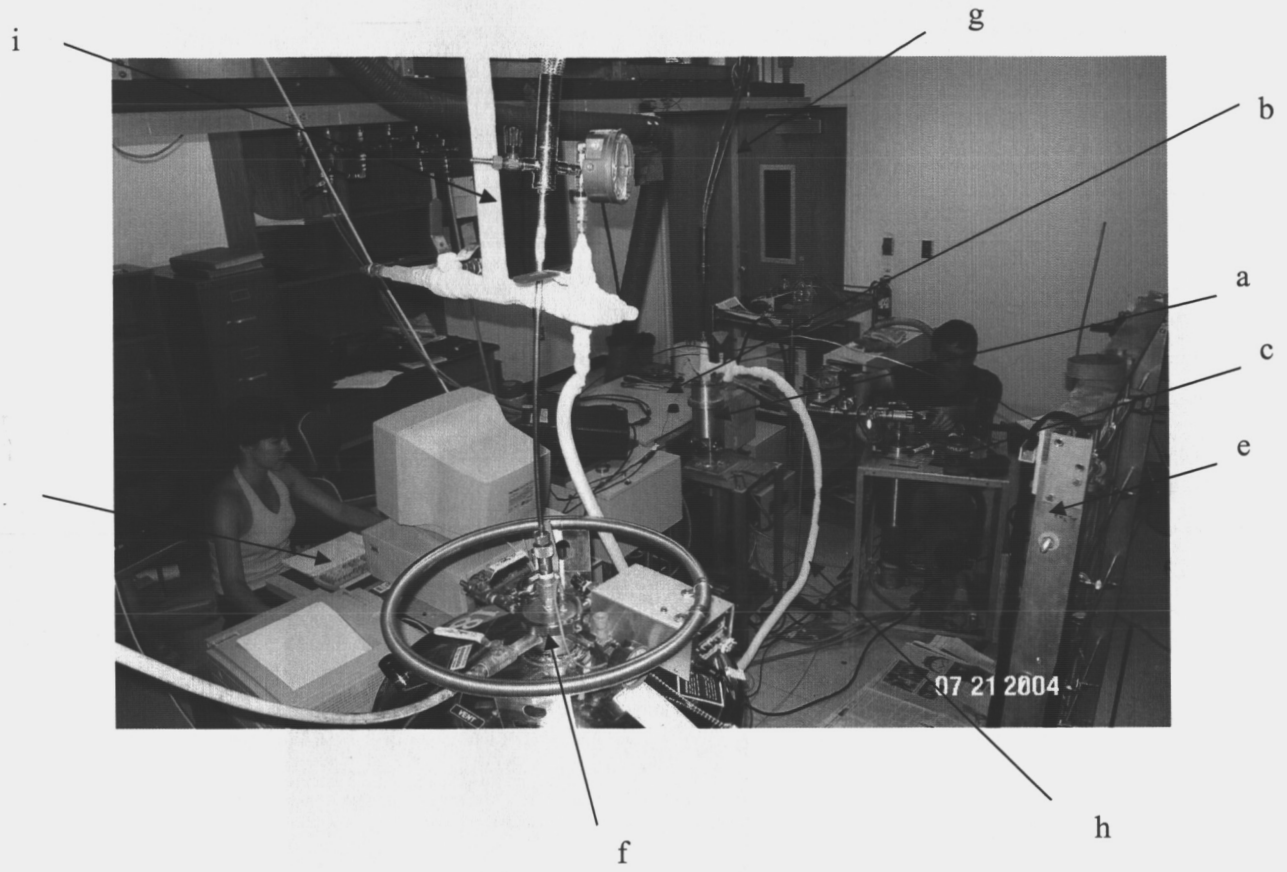

Figure 2. Typical experiment in progress

The cryostat (a) is mounted on a custom made optical bench, which enables consistent positioning of the cryostat relative to the external sampling port of the Bruker infrared spectrometer (b). The movable pumping station (c), consisting of a diffusion pump and a backing rotary pump, is connected to the cryostat via a flexible vacuum line. (d) is the computer console for running the spectrometer and analyzing spectra. (e) is the hydrogen handling and purification system. Liquid helium is transferred from the liquid helium dewar (f) via the flexible transfer line (g) to the cryostat, exhaust gas is collected by the flexible recovery line (h), which is connected to the permanent laboratory recovery system (i). The Nd:YAG laser (j) with steering optics have been temporarily moved aside. The movable pumping station with flexible vacuum line (c) and the flexible recovery line (h) are features, which enable the rotation of the top section of the cryostat and the inner cold finger under cryogenic and high vacuum conditions

UNIVERSITY OF FLORIDA

Figure (3):- Infrared Spectrum of Solid Hydrogen Film at 4 K

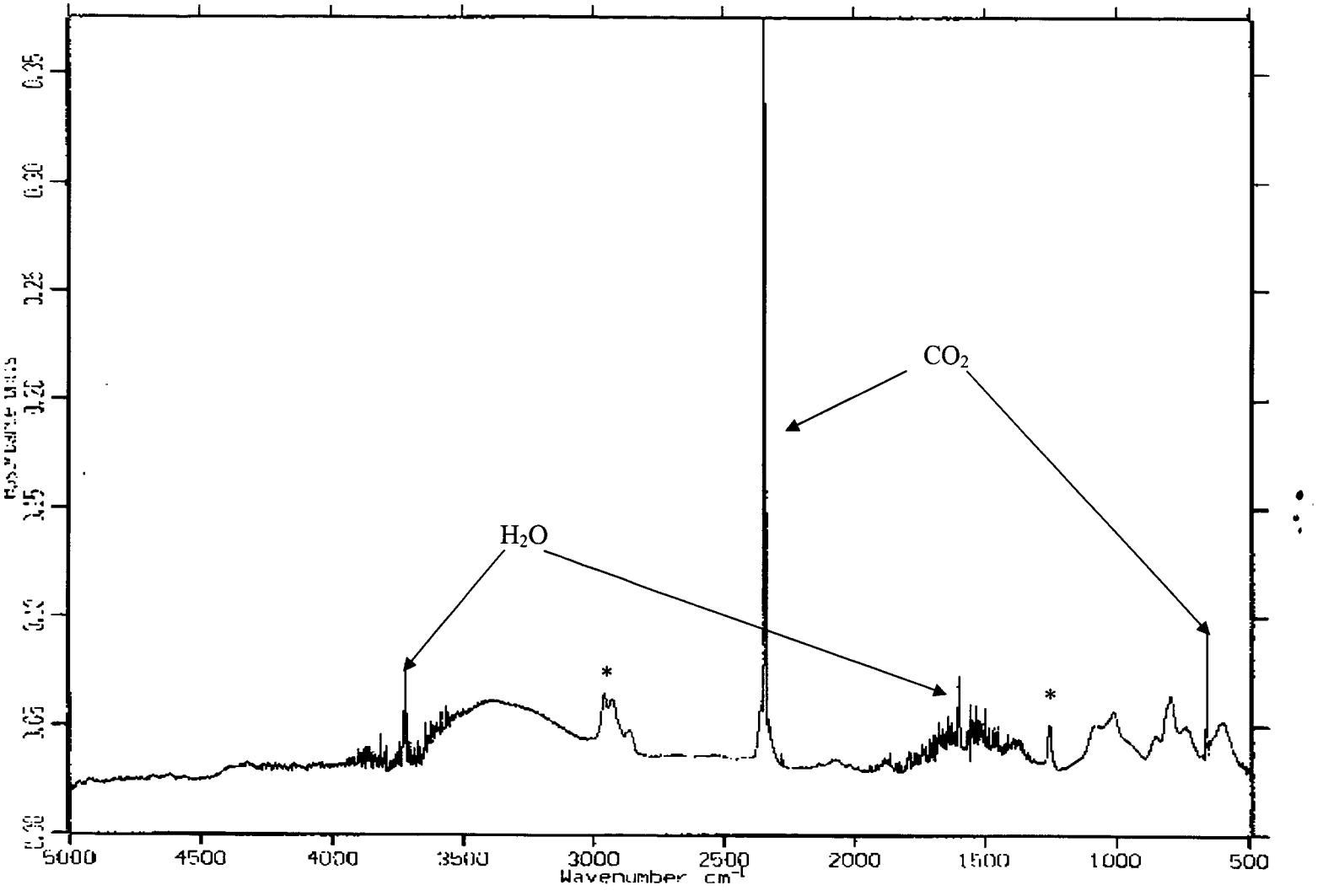

UNIVERSITY OF FLORIDA

Figure (4):- Infrared Spectrum Produced by Laser Ablating Boron and Trapping in Solid Hydrogen at 4 K

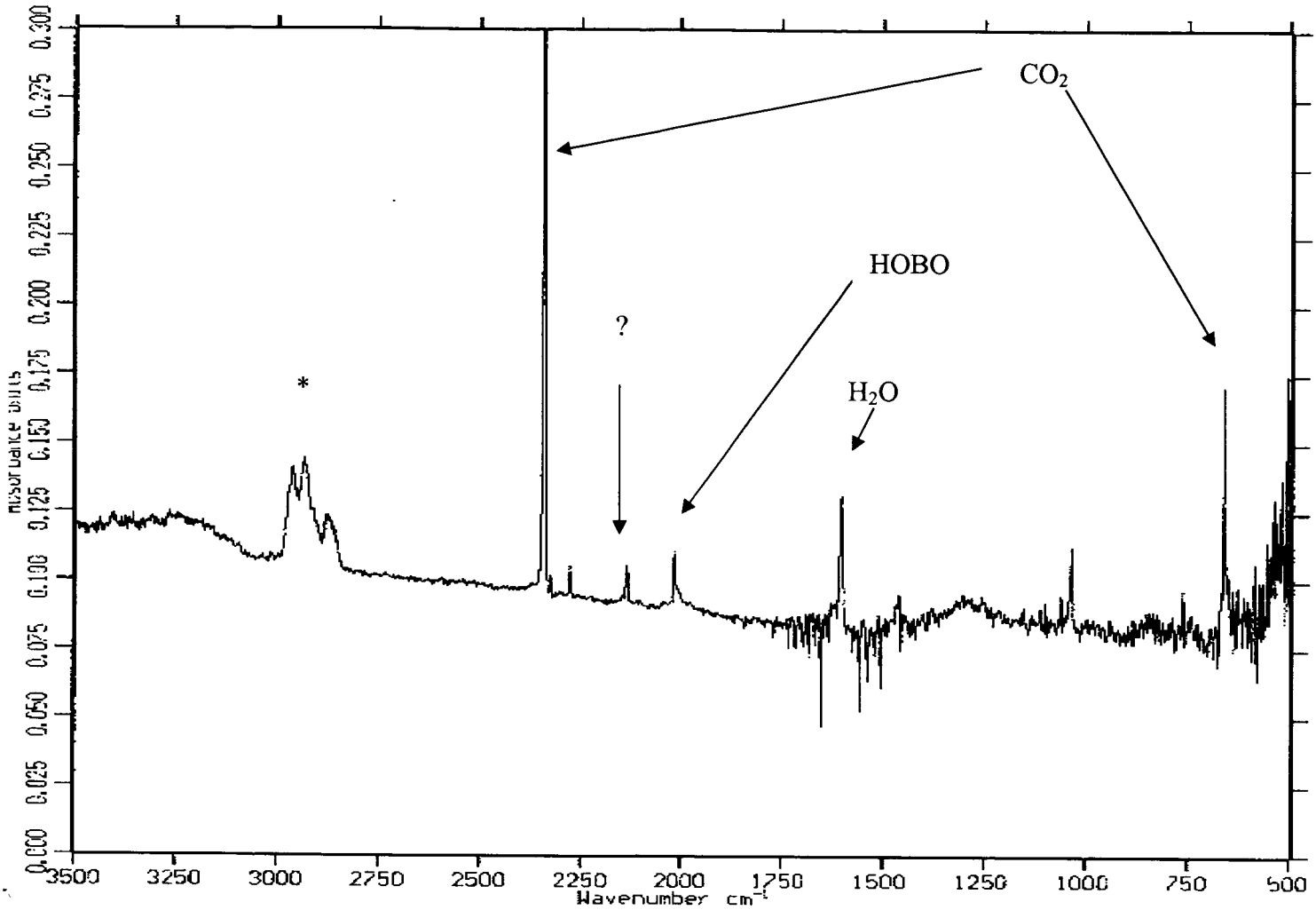

Figure (5):- Infrared Spectrum Produced by Laser Ablating Boron and Trapping in Solid Hydrogen at 4K

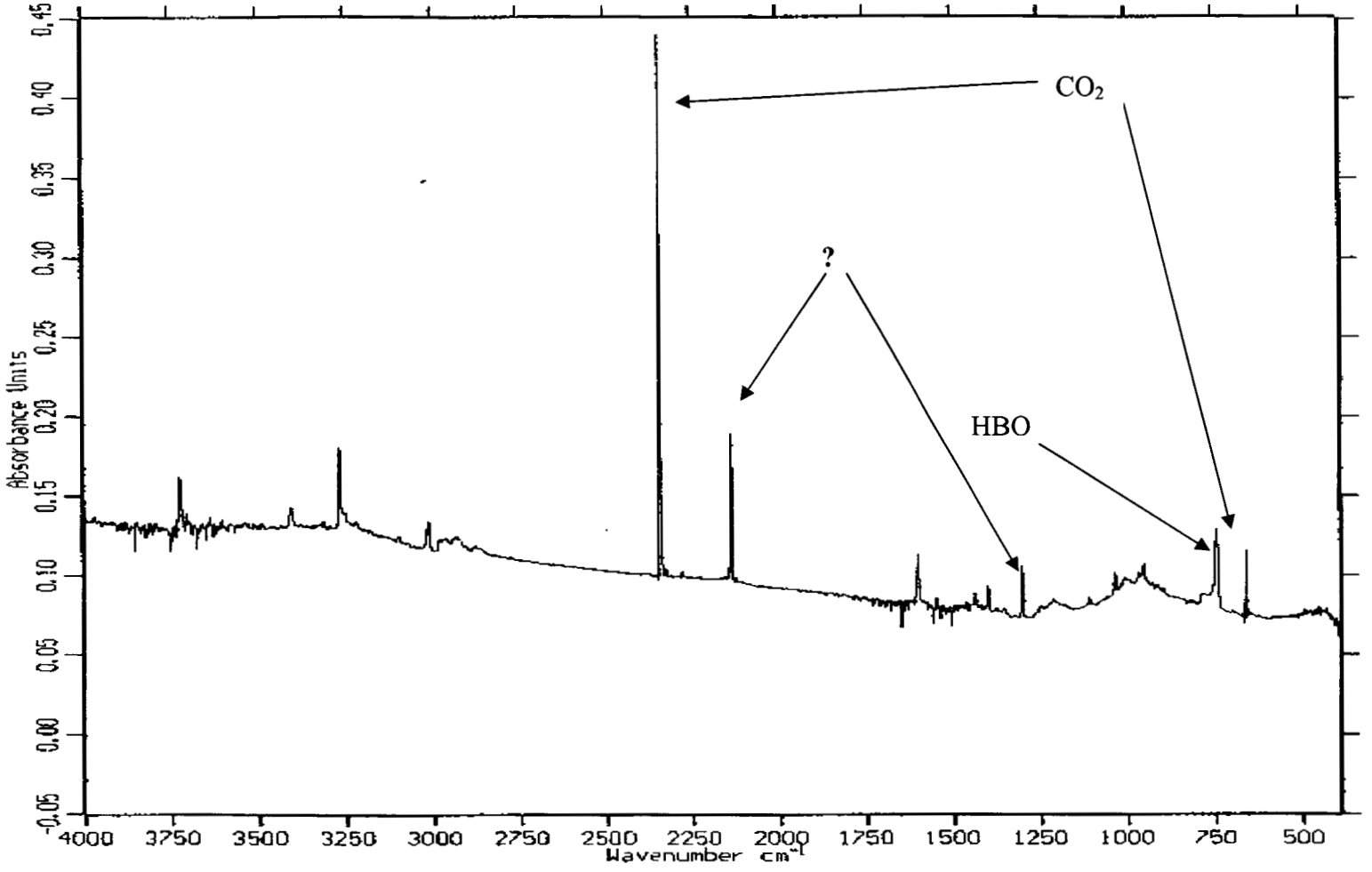

UNIVERSITY OF FLORIDA

Figure (6):- Infrared Spectrum Produced by Laser Ablating Carbon and Trapping in Solid Hydrogen at 4 K